



**DESIGNING EFFICIENT THREE PHASE BRUSHLESS DC MOTOR
CONTROL SYSTEMS**

RAFID IBRAHIM

AGUSTUS 2015

**DESIGNING EFFICIENT THREE PHASE BRUSHLESS DC MOTOR
CONTROL SYSTEMS**

**A THESIS SUBMITTED TO
THE GRADUATE SCHOOL OF NATURAL AND APPLIED
SCIENCES OF
ÇANKAYA UNIVERSITY**

**BY
RAFID IBRAHIM**

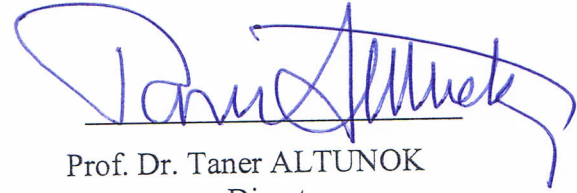
**IN PARTIAL FULFILLMENT OF THE REQUIREMENTS FOR THE
DEGREE OF
MASTER OF SCIENCE
IN
THE DEPARTMENT OF
ELECTRONIC AND COMMUNICATION ENGINEERING**

AGUSTUS 2015

Title of the Thesis: **Designing Efficient Three Phase Brushless DC Motor Control Systems**

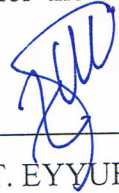
Submitted by **RAFID IBRAHIM**

Approval of the Graduate School of Natural and Applied Sciences, Çankaya University.



Prof. Dr. Taner ALTUNOK
Director

I certify that this thesis satisfies all the requirements as a thesis for the degree of Master of Science.



Prof. Dr. Halil T. EYYUBOĞLU
Head of Department

This is to certify that we have read this thesis and that in our opinion it is fully adequate, in scope and quality, as a thesis for the degree of Master of Science.



Asst. Prof. Dr. Ulaş BELDEK
Supervisor

Examination Date: 17.08.2015

Examining Committee Members

Assoc. Prof. Dr. Orhan GAZI

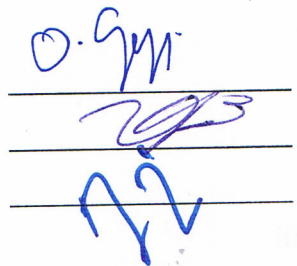
(Çankaya Univ.)

Asst. Prof. Dr. Ulaş BELDEK

(Çankaya Univ.)

Asst. Prof. Dr. Tolga İNAN

(TED Univ.)

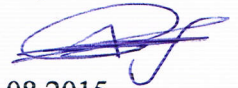


STATEMENT OF NON-PLAGIARISM PAGE

I hereby declare that all information in this document has been obtained and presented in accordance with academic rules and ethical conduct. I also declare that, as required by these rules and conduct, I have fully cited and referenced all material and results that are not original to this work.

Name, Last Name : Rafid, Ibrahim

Signature :



Date :

17.08.2015

ABSTRACT

DESIGNING EFFICIENT THREE PHASE BRUSHLESS DC MOTOR CONTROL SYSTEMS

RAFID IBRAHIM

M.Sc., Department of ELECTRONIC AND COMMUNICATION ENGINEERING

Supervisor: Asst. Prof. Dr. Ulaş BELDEK

AGUSTUS 2015, 44 pages

This thesis presents a mathematical model of three-phase BLDC motor control systems. After the mathematical model open loop system is obtained, it is linearized and a linear approximated model of the plant is obtained. The Linearization enables the synthesis of controllers with high performance, which are realized using the root locus plot of the approximated plant. In the thesis, 3 different controllers are obtained. Two of the controllers are conventional Proportional and Proportional and Integral controllers. The third controller is a FLC controller with two different rule-base settings with sliding mode control strategy. The dynamical characteristics and performance indices of these synthesized controllers are compared as the final step.

Keywords: BLDC Motor, Linearization, Root Locus, PID controllers, FLC controllers.

ÖZ

VERİMLİ ÜÇ FAZLI DOĞRU AKIM MOTOR KONTROL SİSTEMLERİNİN TASARLANMASI

RAFİD İBRAHİM

Yüksek Lisans Elektronik ve Haberleşme Mühendisliği Anabilim Dalı

Tez Yöneticisi: Yrd. Doç. Dr. Ulaş BELDEK

Ağustos 2015, 44 sayfa

Bu tez 3-fazlı Fırçasız Doğru Akım (DA) motor kontrol sistemleri için matematiksel bir model ortaya koymaktadır. Açık döngü sistemin matematiksel modeli elde edildikten sonra, doğrusallaştırma işlemi ile sistemin doğrusal modeli elde edilmiştir. Doğrusallaştırma, doğrusallaştırılmış yaklaşık sistemin kök yereğrisini kullanarak gerçekleştirilen yüksek performanslı denetleyicilerin sentezlenmesine olanak vermiştir. Tezde 3 farklı denetleyici elde edilmiştir. Bu denetleyicilerden 2 tanesi geleneksel oransal ve oransal+integral denetleyicilerdir. Diğer denetleyici ise, 2 farklı kural-tabanı ayarlaması içeren Akan Kipli Denetim stratejisine sahip Bulanık Mantık Denetleyicisidir. Son aşamada, sentezlenen denetleyicilerin dinamik nitelikleri ve performans göstergeleri karşılaştırılmıştır.

Anahtar Kelimeler: : Fırçasız Doğru Akım (DA) Motoru, Doğrusallaştırma, Kök Yereğrisi, Oransal-İntegral-Türevsel Denetleyiciler, Bulanık Mantık Denetleyiciler.

ACKNOWLEDGEMENTS

I would like to express my sincere gratitude to Asst. Prof. Dr. Ulaş BELDEK for his supervision, special guidance, suggestions, and encouragement through the development of this thesis. Also I sincerely thank Prof. Dr. Klaus Werner SCHMIDT for supported me in practice field.

I would like to thank my dear friend Shaheen Salahaldeen for supporting me and stood by me during my studies.

Finally, I would like to express special thank to my wife for her effort and stood by me in all time.

TABLE OF CONTENTS

STATEMENT OF NON-PLAGIARISM.....	iii
ABSTRACT.....	iv
ÖZ.....	v
ACKNOWLEDGEMENTS.....	vi
TABLE OF CONTENTS.....	vii
LIST OF FIGURES.....	iX
LIST OF TABLES.....	Xi
LIST OF ABBREVIATIONS.....	Xii

CHAPTERS:

1. INTRODUCTION.....	1
1.1. Background.....	1
1.2. Application Types of BLDC Motor.....	1
1.3. Review on BLDC Motor Modeling	2
1.4. Comparison of Brushless DC Motor with Traditional DC Motor....	3
1.5. Advantages and Disadvantages of BLDC Motor.....	3
1.6. Review Control of BLDC Motor.....	4
1.7. Thesis Organization.....	5
2. BLDC MOTOR MATHEMATICAL MODEL.....	6
2.1. Principal and Construction BLDC Motor.....	6
2.2. Architecture of the BLDC system.....	6
2.3. BLDC Drives Operation with Inverter.....	8
2.3.1. (2π/3) Angle Switch-On Mode	9
2.3.2. Voltage and Current Control PWM Mode	10
2.4. Rotor Position Sensors.....	11
2.5. BLCD Motor Dynamic Model.....	12

2.6. Current Control: Hysteresis Current Control Technique.....	17
3. CONTROLLERS.....	20
3.1. Type of Controllers.....	20
4. Experimental Results.....	24
4.1. Obtaining the Linearized Open Loop Model of the System.....	25
4.2. PI Controller Design: Root Locus Method.....	26
4.3. P Controller Design: Root Locus Method.....	35
4.4. FLC Controller.....	37
4.5. Comparison of Controllers for Reverse Motor Operation	41
4.6. Comparison of Controllers for Small Reference Changes	41
5. CONCLUSION.....	43
REFERENCES.....	R1
APPENDICES.....	A1
A. CURRICULUM VITAE.....	A1

LIST OF FIGURES

FIGURES

Figure 1	Block diagram of BLDC motor control.....	7
Figure 2	The circuit diagram of the power converter.....	8
Figure 3	Internal Block Diagram off the Power Converter and Controller.....	8
Figure 4	Brushless DC Motor Drive System.....	9
Figure 5	Back-EMF, current waveform and hall position sensor for BLDC motor.....	10
Figure 6	The hall effect sensors in the stator.....	11
Figure 7	The configuration of BLDC motor and voltage source inverter	12
Figure 8	Block diagram for three-phase currents.....	14
Figure 9	Block diagram for speed and torque control.....	17
Figure 10	Hysteresis current control block diagram for phase A.....	18
Figure 11	Block diagram of inverter line-to-line voltages.....	19
Figure 12	The angular velocity control of PMSM motor.....	21
Figure 13	The block diagram of PID controller.....	21
Figure 14	The block diagram of FLC.....	22
Figure 15	The member function distribution of linguistic variables for the inputs and the output of FLC.....	23
Figure 16	The mechanical speed of the open loop system and the approximated systems.....	25
Figure 17	The root locus plot of approximated system at the first alternative.....	27
Figure 18	The root locus plot of the total open loop system together with controller.....	28
Figure 19	The mechanical speed of the motor as a function of time.....	29

FIGURES

Figure 20	Back EMF waveforms for Phases A, B and C respectively	30
Figure 21	Phase currents waveforms for phase A,B and C respectively.....	31
Figure 22	Switching function for Phase a, b and c respectively.....	33
Figure 23	Line-to-line voltages V_{ab} , V_{bc} and V_{ca} respectively.....	34
Figure 24	Equivalent torque of BLDC motor.....	35
Figure 25	Max current of BLDC motor (I_{max}).....	35
Figure 26	The mechanical speed of the motor as a function of time.....	36
Figure 27	Equivalent torque of BLDC motor.....	37
Figure 28	Max current of BLDC motor (I_{max}).....	37
Figure 29	Mechanical speed of FLC case 1.....	38
Figure 30	Equivalent torque of BLDC motor for FLC case 1.....	39
Figure 31	Max current of BLDC motor (I_{max}) of FLC case 1.....	39
Figure 32	Mechanical Speed of FLC Case 2.....	40
Figure 33	Equivalent torque of BLDC motor for FLC case 2.....	40
Figure 34	Max current of BLDC motor (I_{max}) of FLC case 2.....	41

LIST OF TABLES

TABLES

Table 1	Differences of BLDC motor and PMS motor.....	2
Table 2	BLDC Motor Specification.....	24
Table 3	Rule of Fuzzy Logic control case1.....	38
Table 4	Rule of Fuzzy Logic control case2.....	38
Table 5	The performance indices of controllers for -400 rad/sec.....	41
Table 6	The performance indices of controllers for reference changes at lower speeds.....	42
Table 7	The performance indices of controllers for reference changes at higher speeds.....	42

LIST OF ABBREVIATIONS

PMBLDC	Permanent Magnet Brushless DC
PI	Proportional Integral
FLC	Fuzzy Logic Controller
PWM	Pulse Width Modulation
Back- EMF	Back Electromagnetic Force
RPM	Revolutions Per Minute
BLDC	Brushless DC
P	Proportional
PID	Proportional Integral Derivative
PMS	Permanent Magnet Synchronous
E_a, E_b, E_c	back-EMF for each phase
I_a, I_b, I_c	stator currents for each phase
V_{ab}, V_{bc}, V_{ca}	Line to line voltage
V_{dc}	Supply voltage
I_{dc}	Supply current
R_a, R_b, R_c	the stator resistance for each phase
L_a, L_b, L_c	Inductance for each phase
PMAC	Permanent Magnet Alternating Current
$f_a(\theta), f_b(\theta), f_c(\theta)$	The functions of the rotor position
ω_m	the rotor mechanical speed,
K_e	motor voltage constants
T_e	total electromagnetic torque
T_L	load torque
B	damping constant
J	moment of inertia of the motor.
ω_r	Electrical speed

p	Number of poles
θ	rotor position
I_{\max}	Max current
K_t	torque constant of the motor
T_{\max}	Maximum current
t_r	Rise time
t_s	Settling time

CHAPTER 1

INTRODUCTION

1.1 Background

Brushless Direct Current (BLDC) motors are among the motor types, which are becoming popular in recent years. A BLDC motor's stator contains stacked steel laminations [1]. The windings of the motor are wrapped over the slots. The rotor is made of permanent magnets. The number of permanent magnets changes between two to eight pole pairs with north and south poles in an alternating order. The stator windings should be energized in a sequential order in order to operate the BLDC motor properly. Hence it is necessary to know the rotor position in order to understand the winding to be energized at a specific time instant. In the BLDC motor, power transistors are used for changing the polarity, which is performed by switching the transistors in synchronization with the rotor position. BLDC motors often include either internal or external position sensors to sense the actual rotor position.

1.2 Application Types of BLDC Motor

The BLDC motor has been widely used in many applications, we can categorize the applications as:

- **Constant load:** In these applications generally changing the speed is more important and the load is directly connected to the motor shaft. Examples of these kind of loads are fans, pumps and blowers.
- **Varying loads:** In these applications the load of the motor varies depending on time and speed of the motor and they generally require high-speed control accuracy and good dynamic responses. Examples of these devices are compressors, pumps and robot arms.

- **Positioning applications:** Most of the industrial applications come under this category and most of the time the dynamic response of speed and torque characteristics are vital for these applications. Examples of these applications are, mechanical gears and timer belts.

1.3 Review on BLDC Motor Modeling

The BLDC motor and the permanent magnet synchronous (PMS) motor which can be categorized under the permanent magnet motor drives. These motors have the potential to replace induction motor for servo applications [2-3]. The difference between the PMS motor and the BLCD motor is that they have different back electromotive force (back-EMF) characteristics. The PMS motor has a sinusoidal back-EMF whereas the BLDC motor has a trapezoidal back-EMF and besides the stator currents of BLDC motor are nearly rectangular ideally rectangular. The PMS motor and the BLDC motor have a lot of similarities [4]. The differences of these two machines are shown in Table 1.

Table 1: Differences of BLDC motor and PMS motor

	BLDC motor	PMS motor
1	(Back-EMF) is of trapezoidal waveform.	(Back-EMF) is of sinusoidal waveform.
2	Two phases are conducting at a time.	Three phases are conducting at a time.
3	Generated Torque has more ripples.	Generated torque is almost ripple free.
4	Coil span is less than 180 degree, electrical and coil pitch is 1.	Coil span is 180 degree, electrical and coil pitch is greater than 1.
5	Has concentrated winding.	Has distributed winding.

1.4 Comparison of Brushless DC Motor with Traditional DC Motor

In a traditional DC motor, the brushes are used to provide mechanical contact with the supplied electrical source. These contacting materials are called as commutator. This mechanical contact causes an electrical conduction between the armature coil windings and the DC electrical source. The stationary brushes contact with different sections of the rotating commutator as the armature rotates on its axis. The brushes and the commutator acts as a set of electrical switches. Each of these switches are triggered in sequence.

In a BLDC motor, the permanent magnets rotate and the armature coils remains static. The problem is how to transfer current to a moving armature. Replacing the commutator assembly with a controller is one of the methods to solve this problem. The controller which is an embedded circuitry performs the same operation instead of the brushes.

1.5 Advantages and Disadvantage of BLDC Motor

BLDC motors have many advantages over traditional DC motors [5]. A few of these are:

- Higher speed ranges
- Higher efficiency
- Better speed versus torque characteristics
- Long operating life
- Noiseless operation
- Higher dynamic response
- High output power
- Compact volume
- Low maintenance

The main disadvantage of Brushless DC motor is that it is generally more expensive compared to Brushed DC motor due to its permanent magnet and besides it requires complex electronic speed controllers to run.

1.6 Review Control of BLDC Motor

The back-EMF of BLDC motor is trapezoidal they also produce rectangular stator currents. These motors usually require hysteresis current control or pulse width modulation (PWM) current control techniques to adjust the shapes and magnitudes of the stator current [6-7]. In most of the previous studies some significant steady-state analysis has been performed successfully. However in order to design very effective controllers, mathematical model of the system is necessary and without this mathematical model designing an efficient BLDC motor control system is difficult and fails to exhibit an improvement in the performance. In practice, the design of the BLDC motor drive requires some complex tasks to be completed such as devising of control scheme, modeling, simulation and parameters adjustment. The proportional integral (PI) controllers are generally suitable for the linear motor control and they have been widely proposed for BLDC motors. But in practice, many non-linear factors influence the BLDC motors. Most of the time these non-linear factors are due to the driver and the load. In order to prevent these side effects appropriate controllers for speed control are necessary by fine-tuning of controller parameters. Usually PI controllers are applied for speed control applications in permanent magnet motors. In industry, conventional PI controllers are preferred due to ease of implementation and as they possess simple control structure. The drawback of PI controllers arises when there are some control complexities like nonlinearities, parametric variations and load disturbances. One of the drawbacks of PI controllers is that they are more efficient when a linear mathematical model of the system is available. Unfortunately, the permanent magnet BLDC machine has a nonlinear model and for this reason it is not very suitable for linear PI controllers if a fine-tuning of the controller parameters is not carried out. In such circumstances using Fuzzy Logic Controllers (FLC) can be helpful as they are sensitive to parameters changes and robust to disturbances due to varying loads. In addition, FLCs could be easily implemented. Due to these properties it is planned to use a FLC for the BLDC motor and compare its performance with a P or PI controller in this thesis. However in order to implement P or PI controllers a dynamical model of the BLDC motor is also necessary. Hence in order to obtain

good parameter tuning for P and PI controllers we have also modeled the system using its step response.

The contributions of this thesis are as follows:

- A dynamical model (linearized system's transfer function) for the BLDC motor is constructed.
- Depending on this dynamical model P and PI controllers are implemented
- A FLC controller model is implemented and using this model two different sliding mode control strategies (by the application of two different rule bases) are performed.
- The performances of controllers are tested for mechanical angular speed control applications depending on different performance indices.

1.7 Thesis Organization

The thesis contains five chapters. The organization of the thesis is as follows: The second chapter describes the mathematical model of a Permanent Magnet Brushless DC (PMBLDC) motor. In the third chapter the mathematical model of PID controller is introduced and the working principles of FLC are explained. The fourth chapter includes the linear modeling of the non-linear PMBLDC motor system. Depending on this linearized model PI and P controllers are implemented for angular speed control using the root locus design method. Besides the performance of FLC with two different rule-base structures is also tested for angular speed control application. In the last chapter conclusions and future work are emphasized.

CHAPTER 2

BLDC MOTOR MATHEMATICAL MODEL

2.1 Principal and Construction BLDC Motor

Similar to nearly all other types of motors, BLDC motor has two important components: the rotor part and the stator part. BLDC motor can be categorized as DC motor that is turning inside out, so that the armature is on the stator side and the permanent magnet is on the rotor side. It can also be categorized as a permanent magnet AC motor whose torque-current characteristics resembles the DC motor. In a BLDC motor, electronic commutation is used. Besides, the armature lie on the stator, hence the heat produced in the motor is trivially removed away from the windings and the cooling facility of the motor is provided automatically.

In BLDC motors it is important to precisely determine the position of the rotor since the commutation is performed electronically due to the rotor position. Optical position sensors might be for this purpose. Optical position sensors consist of a light source and phototransistors' revolving shutters and its output of is generally a logical signal.

2.2 Architecture of the BLDC system

The block diagram of a BLCD motor control system is shown in the Figure 1. The block diagram contains four main parts. These parts are the power converter, controller, motor and sensors.

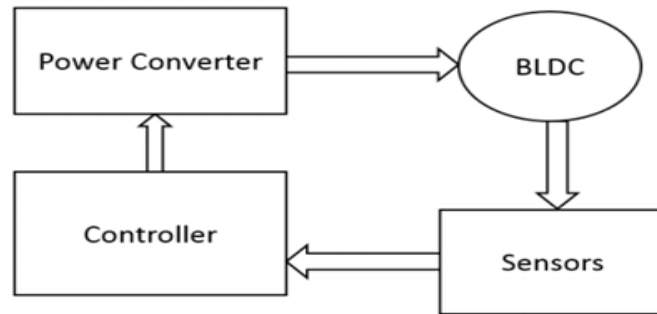


Figure 1 Block diagram of BLDC motor control

In Figure 2 the circuit diagram of the power converter is given. The power converter consists of a three-phase power semiconductor bridge. The main task of the power converter is to transform DC power from the DC source to a balanced three-phase AC power. This AC power is used to convert electrical energy to mechanical energy. In order to operate the BLDC motor the controller needs feedback information about the rotor position [9]. The controller generates signals, which drive the power converter by using a pulse width modulation (PWM) modulator. The internal block diagram of the power converter and controller is shown in Figure 3. In BLDC motor the rotor speed and supplied voltage are directly proportional. In a PWM controller, the PWM duty cycle controls the voltage [8]. When the voltage is applied, a current flows through the windings of the motor and this current generates torque in order to spin the motor. The motor can spin either in clockwise or counterclockwise direction depending on polarity of the applied voltage. The sensors are used to determine the rotor position and this information is also sent to the controller.

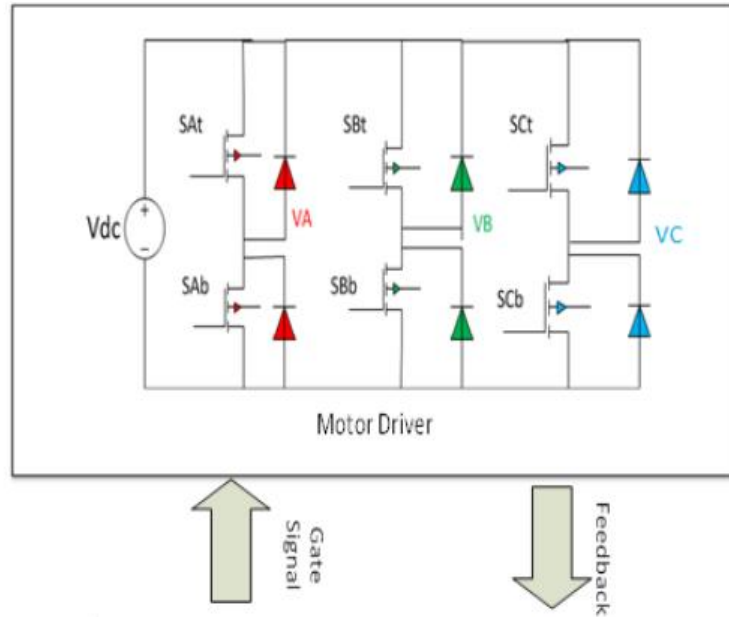


Figure 2 The circuit diagram of the power converter [9]

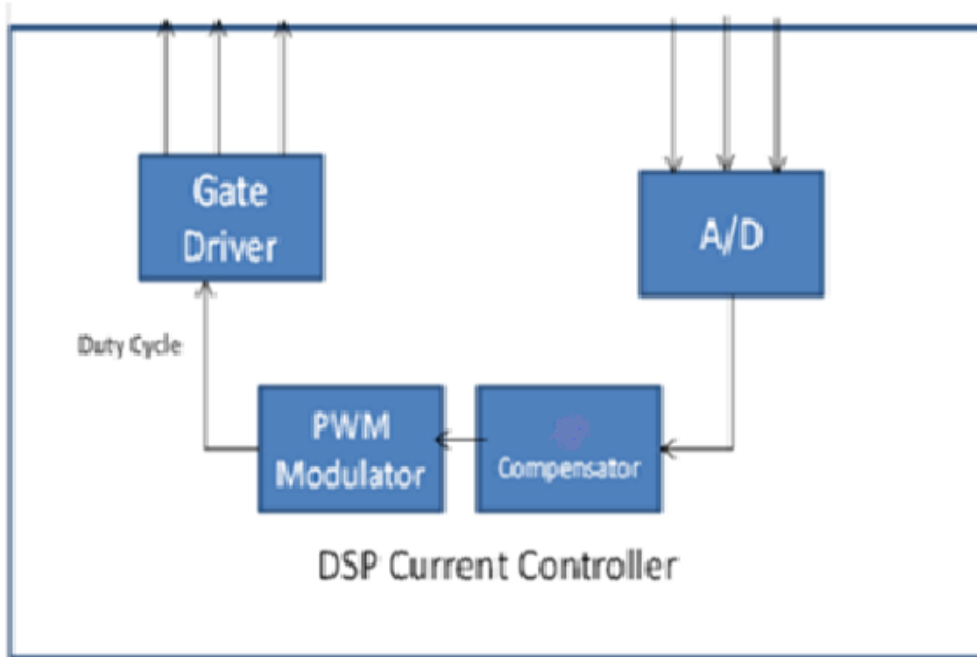


Figure 3 Internal Block Diagram of the Power Converter and Controller [9]

2.3 BLDC Drives Operation with Inverter

The circuit diagram of a BLCD motor with controller and power source inverter is shown in Figure 4. The inverter in self-control mode acts as an electronic

commutator. The position sensors send logical pulses to the inverter and make it function. This kind of motor drive is known as an electronically commutated motor. Two modes of operation is widely used for the inverter:

- $(2\pi/3)$ angle switch-on mode.
- Voltage and current control PWM mode.

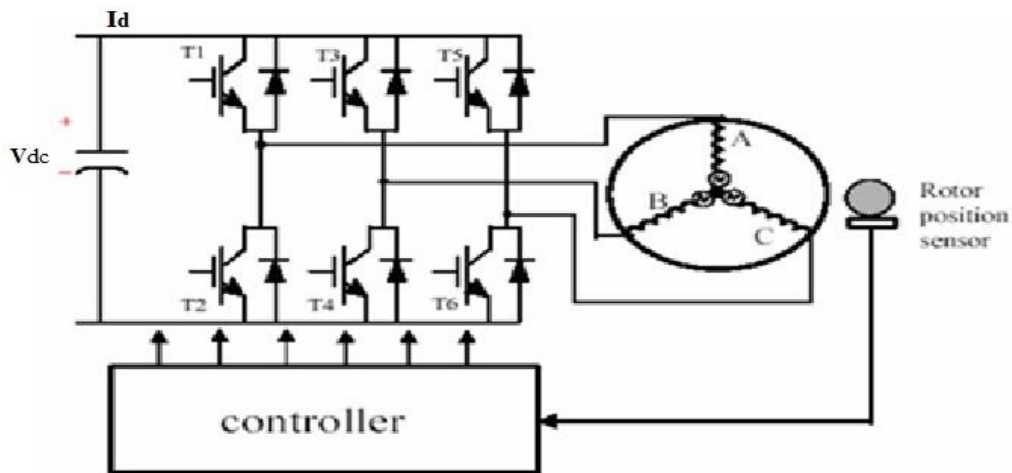


Figure 4 Brushless DC Motor Drive System [10]

2.3.1. $(2\pi/3)$ Angle Switch-On Mode

Inverter operation in the $(2\pi/3)$ angle switch-on mode is shown in Figure 5 [10]. In this figure the waveforms for the back-EMF (E_a , E_b , E_c), the currents through each phases (I_a , I_b , I_c) and the corresponding position sensor logic values (Hall A, Hall B, Hall C) are demonstrated depending on varying angles of the motor shaft position. There are six switches of the inverter (T1 –T6) and these switches work in accordance with these waveforms. As the result of this sequential operation, the input currents I_a , I_b and I_c resemble square waves. These square waves are activated in a sequence such that there is $(2\pi/3)$ phase difference between each other. It is observed that for obtaining such a sequence of waveforms two switches should be on at any time instant, one from the upper group (either T1 or T3 or T5) and other one from the lower group (either T2 or T4 or T6) while the remaining switches should be off (see Figure 4). Assume at a specific time instant t_1 , only the switches T1 and T6 are on and the other switches are all off, the supply voltage is V_{dc} and current is I_{dc} . In this

time instant the current I_{dc} will flow from phase A to phase C as these phases are in series due to switches' configuration. Assume at time instant t_2 , which is reached after a phase change of $\pi/3$, switch T6 is turned off and switch T4 is turned on while switch T1 is still on. In this case the input current will flow from phase A to phase B.

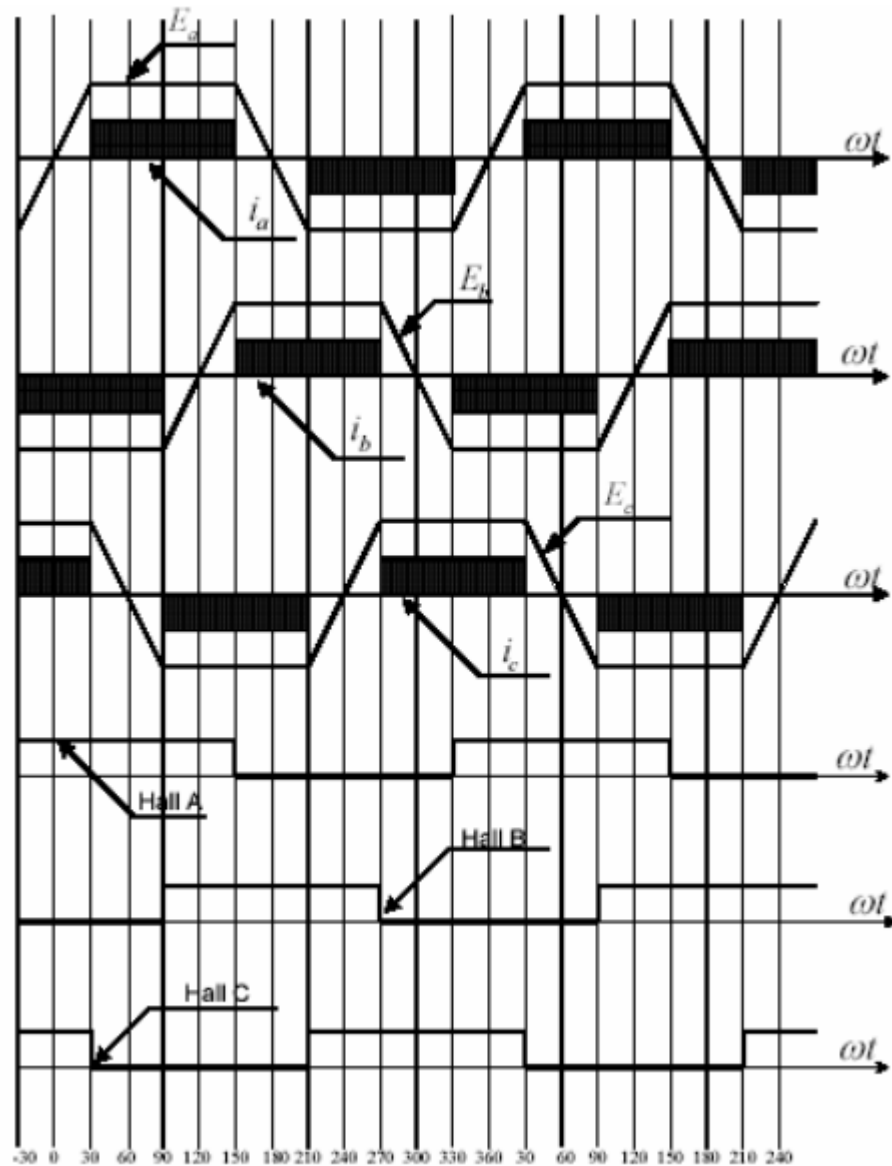


Figure 5 Back-EMF, current waveform and hall position sensor for BLDC motor [10]

2.3.2. Voltage and Current Control PWM Mode

In Section 2.3.1 the inverter switches were controlled to give commutator function commands just when the devices were sequentially ON-OFF for $(2\pi/3)$ angle duration. Besides this strategy, it is possible to activate the switches in PWM

chopping mode for controlling voltage and current continuously at the machine terminals. There are essentially two chopping modes for current control of the inverter. These modes are freewheeling mode and feedback mode. In both of these modes devices are turned on and off on duty cycle basis to adjust the motor average current and the motor average voltage.

2.4 Rotor Position Sensors

The functionality of Hall Effect sensors depends on the physical phenomenon which is called as Hall Effect: an AC current in a conductor generate magnetic field that works as a transverse force on the moving charge carriers, and hence pushing them to different sides of the conductor (positively charged carriers to one side and negatively charged carrier to the other side of the conductor due to the direction of the magnetic field). Existence of charges at the opposite sides of the conductor will balance this magnetic effect and as a result a measurable transverse voltage will be induced at the different sides of the conductor, which is named as the Hall effect. Edwin Hall discovered this phenomenon in 1879 [11].

BLDC motor commutation is controlled electronically. The motor is rotated through energizing the windings of stator in a particular sequence. In order to sense the rotor position Hall effect sensors are used. The Hall sensors are generally embedded in the stator. In Figure 6 the illustrative positions of the Hall effect sensors replaced in the motor are shown.

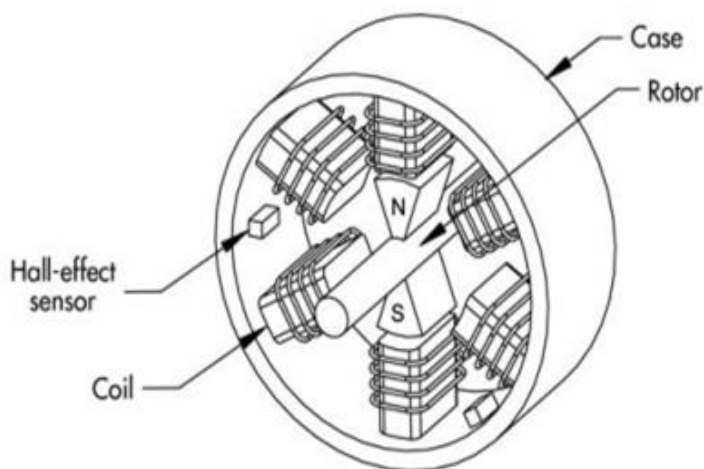


Figure 6 The Hall effect sensors in the stator [9]

At each time the rotor magnetic poles pass through the sensor, a magnet also passes by the same sensor, and hence the sensor changes state at the same angular position. Subsequently, at each time the rotor magnetic poles pass near the Hall sensor, the sensor will send a low or a high signal for the south or north poles to the controller. The exact sequence for commutation can be determined according to the combinations of sensor signals.

2.5. BLCD Motor Dynamic Model

In Figure 7, the BLDC motor electrical model with voltage source inverter is shown. In this model the motor is connected to the output of the inverter, and a constant voltage is supplied to the terminals of the inverter. While constructing the model it is also assumed that there are no power losses in the inverter and the windings of the motor [12]. We have used the BLDC motor model used in [12] for obtaining our mathematical equations.

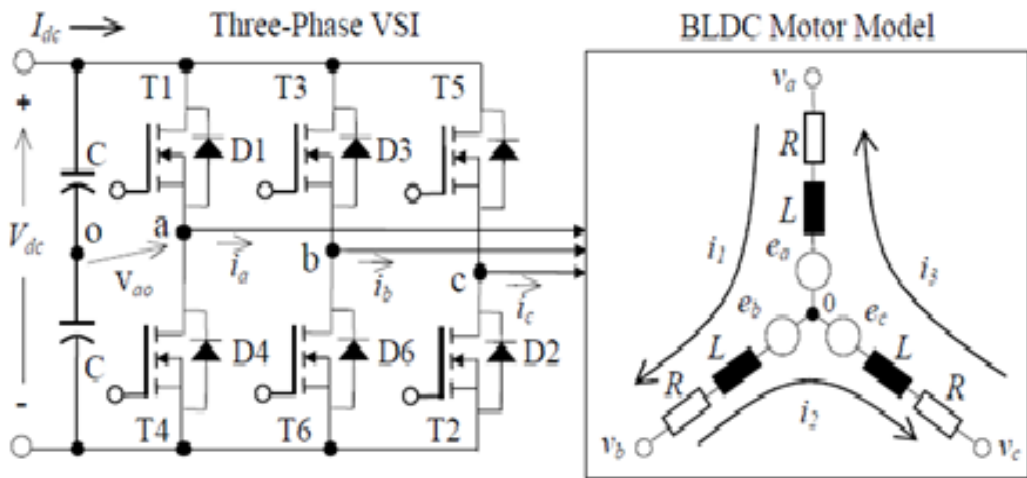


Figure 7 The configuration of BLDC motor and voltage source inverter [12]

We can write the phase voltage equations of BLDC motors as follow:

$$V_a = R_a I_a + L_a \frac{di_a}{dt} + M_{ab} \frac{di_b}{dt} + M_{ac} \frac{di_c}{dt} + e_a \quad (2.1)$$

$$V_b = R_b I_b + L_b \frac{di_b}{dt} + M_{ba} \frac{di_a}{dt} + M_{bc} \frac{di_c}{dt} + e_b \quad (2.2)$$

$$V_c = R_c I_c + L_c \frac{di_c}{dt} + M_{cb} \frac{di_b}{dt} + M_{ca} \frac{di_a}{dt} + e_c \quad (2.3)$$

In these equations V_a , V_b and V_c are the respective phase voltages of the windings I_a , I_b and I_c are the stator currents for each phase, R_a , R_b and R_c are the stator resistance values per phase, M_{ab} , M_{ba} , M_{bc} , M_{cb} , M_{ac} and M_{ca} represent mutual inductance values between each phase and L_a , L_b and L_c stand for self inductance values per each corresponding phases.

We can assume that:

$$L_a = L_b = L_c = L$$

and

$$M_{ab} = M_{ba} = M_{ac} = M_{ca} = M_{bc} = M_{cb} = M$$

As the windings are symmetrical and identical.

We can also take

$$R_a = R_b = R_c = R$$

As we are assuming the system is a three phase balanced system.

Using above assumptions we can rewrite Equation 2.1, Equation 2.2 and Equation (2.3) as follow:

$$V_a = RI_a + L \frac{dI_a}{dt} + M \frac{dI_b}{dt} + M \frac{dI_c}{dt} + e_a \quad (2.4)$$

$$V_b = RI_b + L \frac{dI_b}{dt} + M \frac{dI_a}{dt} + M \frac{dI_c}{dt} + e_b \quad (2.5)$$

$$V_c = RI_c + L \frac{dI_c}{dt} + M \frac{dI_b}{dt} + M \frac{dI_a}{dt} + e_c \quad (2.6)$$

Neglecting the mutual inductance values (M) from the Equations 2.4, 2.5 and 2.6 we obtain:

$$V_a = RI_a + L \frac{dI_a}{dt} + e_a \quad (2.7)$$

$$V_b = RI_b + L \frac{dI_b}{dt} + e_b \quad (2.8)$$

$$V_c = RI_c + L \frac{dI_c}{dt} + e_c \quad (2.9)$$

We can combine Equations 2.7, 2.8 and 2.9 in a matrix as follow:

$$\begin{bmatrix} V_a \\ V_b \\ V_c \end{bmatrix} = \begin{bmatrix} R & 0 & 0 \\ 0 & R & 0 \\ 0 & 0 & R \end{bmatrix} \begin{bmatrix} I_a \\ I_b \\ I_c \end{bmatrix} + \begin{bmatrix} L & 0 & 0 \\ 0 & L & 0 \\ 0 & 0 & L \end{bmatrix} \frac{d}{dt} \begin{bmatrix} I_a \\ I_b \\ I_c \end{bmatrix} + \begin{bmatrix} e_a \\ e_b \\ e_c \end{bmatrix} \quad (2.10)$$

Using Equation (2.10) we can also find,

$$\begin{aligned}
V_{ab} - e_{ab} &= R(I_a - I_b) + L \frac{d}{dt} (I_a - I_b) \\
V_{bc} - e_{bc} &= R(I_b - I_c) + L \frac{d}{dt} (I_b - I_c) \\
V_{ca} - e_{ca} &= R(I_c - I_a) + L \frac{d}{dt} (I_c - I_a)
\end{aligned}
\tag{2.11}$$

Defining the loop currents as I_1 , I_2 and I_3 , we can also write

$$\begin{aligned}
I_a &= I_1 - I_3 \\
I_b &= I_2 - I_1 \\
I_c &= I_3 - I_2
\end{aligned}
\tag{2.12}$$

In Figure 8, block diagram for generation of the phase currents I_a , I_b and I_c is shown.

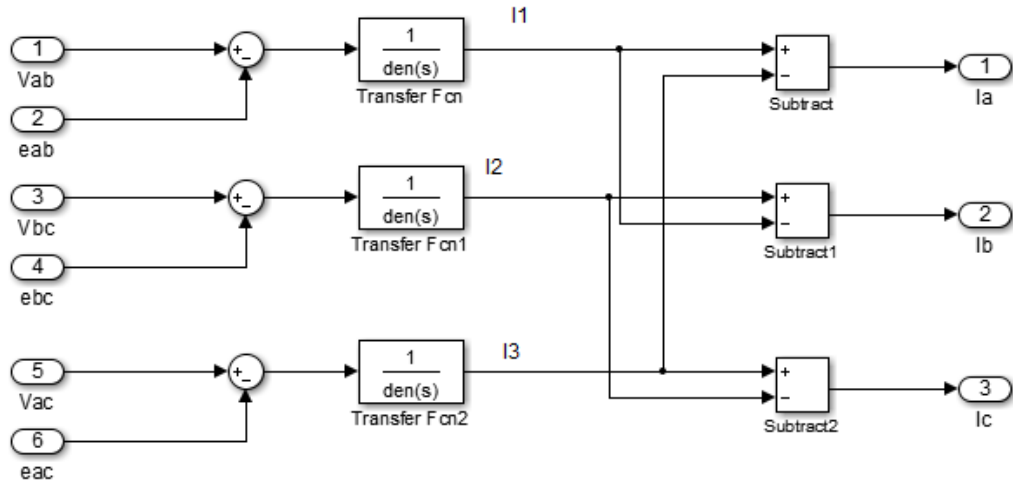


Figure 8 Block diagram for phase currents.

As only two phases are excited through a conduction period, Equation in 2.11 can be rewritten as,

$$\begin{aligned}
V_{ab} - e_{ab} &= 2RI_1 + 2L \frac{dI_1}{dt} \\
V_{bc} - e_{bc} &= 2RI_2 + 2L \frac{dI_2}{dt} \\
V_{ca} - e_{ca} &= 2RI_3 + 2L \frac{dI_3}{dt}
\end{aligned}
\tag{2.13}$$

In terms of functionality BLDC motors are generally put in the category of Permanent Magnet Alternating Current (PMAC) motors. PMAC motors can be grouped into two types. The first type is represented as permanent magnet synchronous motor (PMSM). This motor produce sinusoidal back-EMF and it must be supplied with sinusoidal current / voltage source. The second type is BLDC motor

and it has trapezoidal back-EMF. The back-EMF voltage is produced over the windings of the motor, while the motor is rotating. The polarity of back-EMF is in reverse direction compared to the corresponding phase voltage. Basically back-EMF depends on three factors, magnetic field generated by rotor magnets, mechanical angular velocity of the rotor and the number of turns in the stator windings. Hence, the produced trapezoidal back-EMFs for each phase are functions of the rotor position, and mathematically they can be written as [13-14]:

$$\begin{aligned}
 e_a &= f_a(\theta)K_e w_m \\
 e_b &= f_b(\theta)K_e w_m \\
 e_c &= f_c(\theta)K_e w_m
 \end{aligned} \tag{2.14}$$

In Equation 2.14, θ represented the rotor electrical position, w_m represents the rotor mechanical speed, $f_a(\theta)$, $f_b(\theta)$ and $f_c(\theta)$ are the functions of rotor position and K_e is the motor voltage constants for each phase. The modeling of the back-EMF waveforms is implemented according to the assumption that all three phases have identical trapezoidal periodical back-EMF waveforms with 120 degrees phase difference between each of them. The functions of the rotor position $f_a(\theta)$, $f_b(\theta)$ and $f_c(\theta)$ in a single period can be represented using the equations below:

$$f_a(\theta) = \left\{ \begin{array}{ll} \left(\frac{6}{\pi}\right)\theta & 0 < \theta < \frac{\pi}{6} \\ 1 & \frac{\pi}{6} < \theta < \frac{5\pi}{6} \\ -\left(\frac{6}{\pi}\right)\theta + 6 & \frac{5\pi}{6} < \theta < \frac{7\pi}{6} \\ -1 & \frac{7\pi}{6} < \theta < \frac{11\pi}{6} \\ \left(\frac{6}{\pi}\right)\theta + 12 & \frac{11\pi}{6} < \theta < 2\pi \end{array} \right\} \tag{2.15}$$

$$f_b(\theta) = \left\{ \begin{array}{ll} -1 & 0 < \theta < \frac{\pi}{2} \\ \left(\frac{6}{\pi}\right)\theta - 4 & \frac{\pi}{2} < \theta < \frac{5\pi}{6} \\ 1 & \frac{5\pi}{6} < \theta < \frac{9\pi}{6} \\ -\left(\frac{6}{\pi}\right)\theta + 10 & \frac{9\pi}{6} < \theta < \frac{11\pi}{6} \\ -1 & \frac{11\pi}{6} < \theta < 2\pi \end{array} \right\} \tag{2.16}$$

$$f_c(\theta) = \left\{ \begin{array}{ll} 1 & 0 < \theta < \frac{\pi}{6} \\ -\left(\frac{6}{\pi}\right)\theta + 2 & \frac{\pi}{6} < \theta < \frac{\pi}{2} \\ -1 & \frac{\pi}{2} < \theta < \frac{7\pi}{6} \\ \left(\frac{6}{\pi}\right)\theta - 8 & \frac{7\pi}{6} < \theta < \frac{9\pi}{6} \\ 1 & \frac{9\pi}{6} < \theta < 2\pi \end{array} \right\} \quad (2.17)$$

$f_a(\theta)$, $f_b(\theta)$ and $f_c(\theta)$ can take values between 1 and -1.

We know that the torque produced per phase is directly proportional with the phase current and back-EMF and inversely proportional with the mechanical angular velocity of the motor. Hence torque produced at each phase can be written as:

$$\begin{aligned} T_a &= \frac{e_a \times I_a}{w_m} \\ T_b &= \frac{e_b \times I_b}{w_m} \\ T_c &= \frac{e_c \times I_c}{w_m} \end{aligned} \quad (2.18)$$

The total electromagnetic torque is the result of summation of the torques produced at each phase. Thus we obtain,

$$T_e = T_a + T_b + T_c \quad (2.19)$$

In Equation 2.19, T_e is the total electromagnetic torque. The equation of motion for the BLCD motor can be written as,

$$\frac{dw_m}{dt} = \frac{1}{J} (T_e - T_L - BW_m) \quad (2.20)$$

In Equation 2.20, T_L is the load torque, B is the damping constant and J is the moment of inertia of the motor. The relation between the mechanical angular speed of the motor and the electrical angular frequency of the motor depends on the number of poles found on the motor and it can be written as,

$$w_r = \frac{p}{2} w_m \quad (2.21)$$

In Equation (2.21), w_r is the electrical angular frequency (speed) of the motor and p is the number of poles. In order to find the rotor position vector θ , we can use Equation (2.22) and the figure 9 show who we obtain (θ , I_{\max} , w_r).

$$\frac{d\theta}{dt} = w_r \quad (2.22)$$

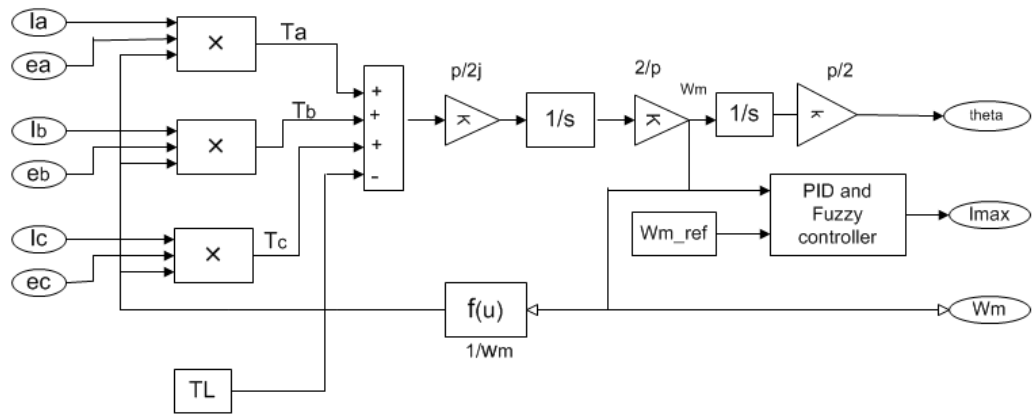


Figure 9 Block diagram for speed and torque control

The mechanical angular speed of the motor is controlled by a control signal, which is the reference torque value T_{max} produced by the controller. This control signal T_{max} is converted to the current value I_{max} (the reference current value) by the torque equation

$$I_{max} = \frac{T_{max}}{K_t} \quad (2.23)$$

In Equation 2.23, K_t is the torque constant of the motor.

2.6 Current Control: Hysteresis Current Control Technique

There are mainly two types of current control techniques for the BLDC motor drive. The first one is the duty-cycle controlled voltage PWM technique and the second one is hysteresis current control technique [15]. In our model we preferred using hysteresis current control technique in [16-17]. The mathematical equation for this current control method is explained for one of the phases of the three-phase system (for our model it is done for phase A). Then finding the mathematical equations for the other phases (phase B and Phase C) is trivial since we just have to apply a phase shift of 120 degree for the other phases. The hysteresis current control logic SIMULINK model can be seen in Figure10. As seen from the figure the model has 4 inputs. The first input is u_1 (I_a phase current of phase A). The second input is u_2 (the previous value of phase current I_a). The third input is u_3 (I_{max} the reference current value) and the last input is u_4 (the angular position of motor θ).

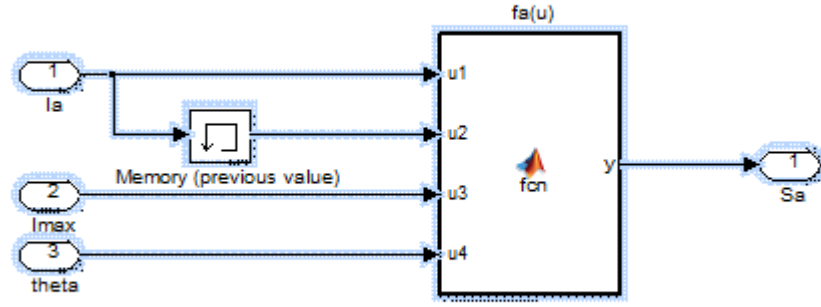


Figure 10 Hysteresis current control block diagram for phase A

The mathematical output of the hysteresis current control block for phase A in Figure 2.8 is [12]

$$S_a = f_a(u) = (U_4 > \pi/6) \times (U_4 < 5\pi/6) \times ((U_1 < U_3 * 0.9) - (U_1 > U_3 * 1.1) + (U_1 > U_3 * 0.9) \times (U_1 < U_3 * 1.1) \times (U_1 > U_2) - (U_1 > U_3 * 0.9) \times (U_1 < U_3 * 1.1) \times (U_1 < U_2)) + (U_4 > 7\pi/6) \times (U_4 < 11\pi/6) \times (-(U_1 > U_3 * 0.9) + (U_1 < U_3 * 1.1) - (U_1 < U_3 * 0.9) \times (U_1 > U_3 * 1.1) \times (U_1 < U_2) + (U_1 < U_3 * 0.9) \times (U_1 > U_3 * 1.1) \times (U_1 > U_2)) \quad (2.24)$$

The details about Equation 2.24 and how this hysteresis current control equation is obtained were deeply analyzed in [12]. Using the hysteresis current control we can obtain the phase voltages as,

$$\begin{aligned} V_a &= \frac{V_{dc}}{2} \times S_a \\ V_b &= \frac{V_{dc}}{2} \times S_b \\ V_c &= \frac{V_{dc}}{2} \times S_c \end{aligned} \quad (2.25)$$

In Equation 2.25, S_a , S_b and S_c are the outputs of the hysteresis control blocks and V_{dc} is the supplied DC voltage to the power converter circuit. Using Equation 2.25 we can also obtain the inverter line-to-line voltages,

$$\begin{aligned} V_a - V_b &= V_{ab} = \frac{V_{dc}}{2} \times (S_a - S_b) \\ V_b - V_c &= V_{bc} = \frac{V_{dc}}{2} \times (S_b - S_c) \\ V_c - V_a &= V_{ca} = \frac{V_{dc}}{2} \times (S_c - S_a) \end{aligned} \quad (2.26)$$

In Equation 2.26 V_{ab} , V_{bc} and V_{ca} are the line-to-line voltages of the inverter circuit.

In Figure 11, there is the block diagram for the generation of line-to-line voltages.

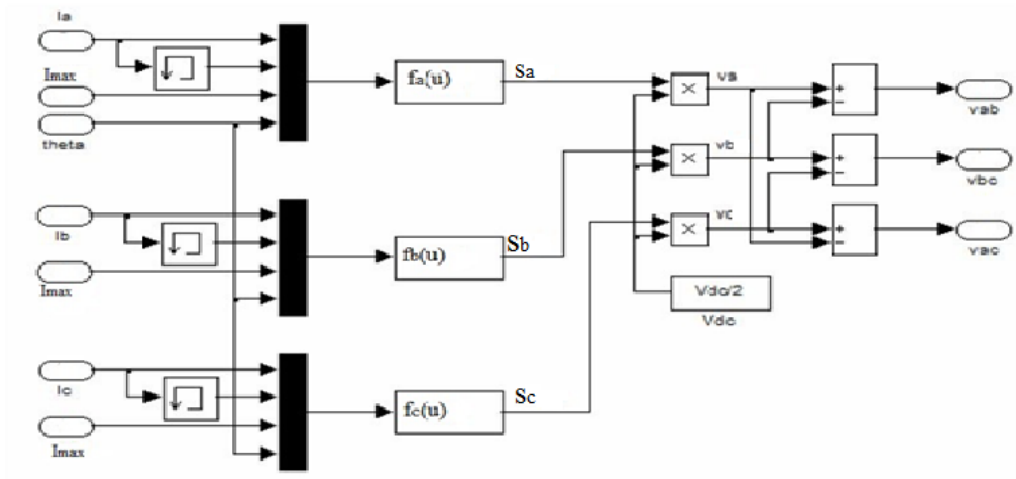


Figure 11 Block diagram of inverter line-to-line voltages

CHAPTER 3

CONTROLLERS

3.1 Type of Controllers

Because of the problems encountered while in operation which are generally instability or their fast dynamics, dynamical systems require a suitable control strategy in order to achieve stability and in order to function in desired conditions. Due to their non-linear characteristics and partially due to external effects such as disturbance and load, the velocity and position control of electric motors are critical issues depending on the requirements of handled process [18]. The position of the motor is the degree of the rotation of the motor shaft and the angular velocity (speed) of the motor is the amount of change in the motor position with respect to time. Generally these two entities should be adjusted precisely in most of the industrial applications. The method to adjust these entities is using feedback control: The set point value and current value of the controlled output are compared with each other and an error signal is obtained. Depending on the error signal, the controller produces the control signal (command signal which is the input of the plant). The control signal drives the plant and thus changes the current value of the controlled output. An illustrative diagram of angular speed (velocity) control for a Permanent Magnet BLDC motor using feedback control is given in Figure12 [19]. In this figure, the entity to be controlled is the angular speed of the motor w_m . It is compared with the reference set-point value w_{m_ref} , and the error signal e is obtained. The controller produces the reference current value I_{max} due to this error signal e and I_{max} gets into the plant and changes the current value of the angular speed.

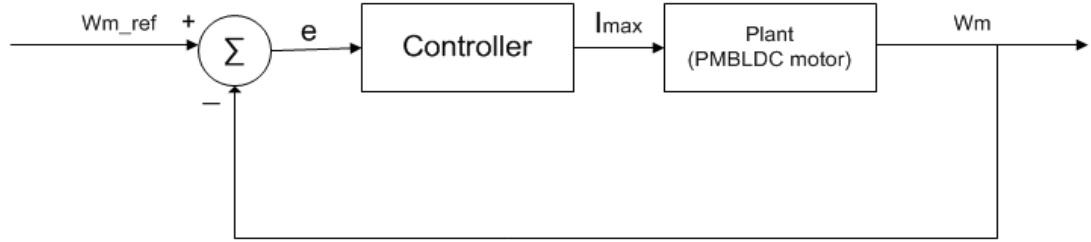


Figure 12 The angular velocity control of PMBLDC motor

In the applications in Chapter 4, we have used two different types of controllers with different parameter settings in order to adjust the mechanical angular speed of the motor to desired set-point value. The first controller type is a PID (proportional-integral-derivative) controller. The block diagram of this controller is given in Figure 13.

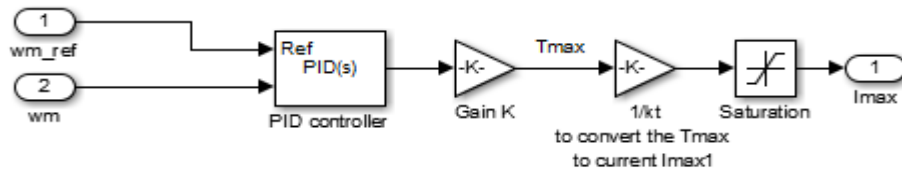


Figure 13 The block diagram of PID controller

The mathematical equations of the PID controller block in Figure 13 are,

$$e(t) = w_{m_ref}(t) - w_m(t) \quad e \quad (3.1)$$

$$T_{max} = K \left(P e(t) + D \frac{de(t)}{dt} + I \int e(t) dt \right) \quad (3.2)$$

$$I_{max} = \frac{T_{max}}{K_t} \quad (3.3)$$

In Equations 3.1, 3.2 and 3.3, P is the proportional, D is the derivative, I is the integral and K is the general gain parameters [20-21]. Sometimes K can be also inserted implicitly into P, I and D by simply multiplication. $e(t)$ is the error signal, T_{max} is the reference torque value, which is the output of controller, K_t is the torque constant and I_{max} is the reference current value supplied to the motor. In applications in order not to let the reference current value exceed very high critical values and

damage the motor it is passed through a saturation block in the simulations. The limit values of the saturation block are taken as 40 and -40 Ampere (≈ 6 times the rated current value of the motor). There are various methods to adjust the parameters of PID controller. Some of those methods are applied in Chapter 4. However adjusting D parameter is demanding and it requires extra effort, even optimization might be necessary. Luckily, adjusting K, P and I are straightforward by using some conventional techniques some of which are applied in Chapter 4.

The second controller we used in the simulations is a Fuzzy Logic Controller (FLC) [22-23-24]. The block diagram of the FLC is shown in Figure 14.

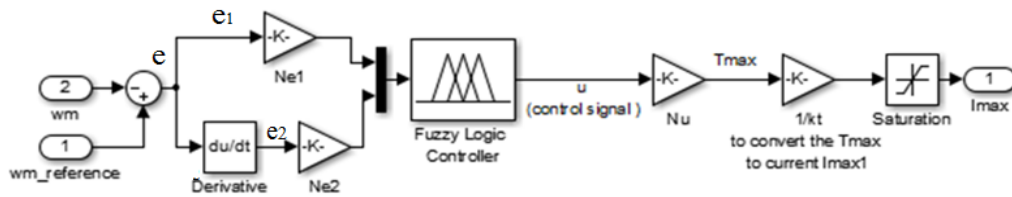


Figure 14 The block diagram of FLC.

FLC takes two inputs. These inputs are the error signal e (will be called as e_1 after this point) and derivative of the error signal e_2 . The inputs are multiplied by normalization factors N_{e1} and N_{e2} respectively and then applied to FLC. The output of FLC is u (the control command) and it is also multiplied by another normalization factor N_u to scale the output to a value suitable for the terminal control element T_{max} . FLC enclose a rule-base structure and the rules of the rule-base structure are of the form:

IF e_1 is at t_{e1} AND e_2 is at t_{e2} THEN u is at t_u

In this rule, att_{e1} is the attribute of the input e_1 , at t_{e2} is the attribute of input e_2 and at t_u is the attribute of the output u . The attributes of FLC are assigned some linguistic variables such as Positive Big (PB), Positive Medium (PM), Positive Small (PS), Zero (Z), Negative Small (NS), Negative Medium (NM), Negative Big (NB). For the inputs and the output of the FLC, each linguistic variable has a membership function distribution. The distribution of the membership functions for the inputs e_1 and e_2 and the output u is shown in Figure 15.

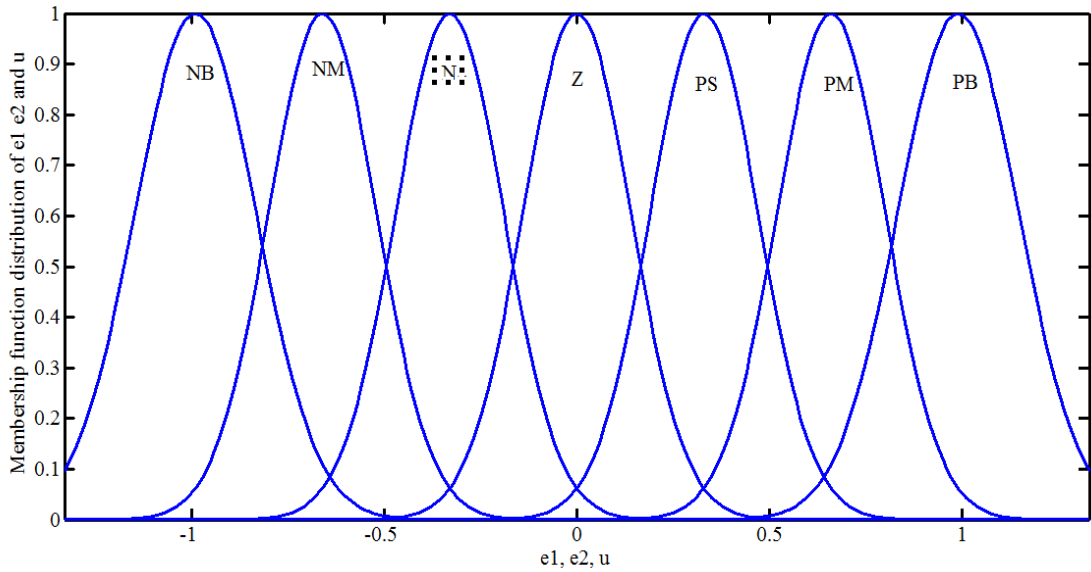


Figure 15 The member function distribution of linguistic variables for the inputs and the output of FLC

The input e_1 and e_2 are passed through a fuzzification process and they are assigned a linguistic variable together with the membership value. After this step, a fuzzy inference mechanism is carried out using the rules in the rule-base [25]. Finally by defuzzification process, a crisp output value u is obtained. There are many different types of inference mechanisms and defuzzification processes. The ones used in our simulations in Chapter 4 are min-max type compositional rule inference mechanism and centroid method for defuzzification.

As done in the PID controller, using Equation 3.3 the reference torque T_{\max} value is also converted into the reference current value I_{\max} through the saturation block

CHAPTER 4

Experimental Results

We implemented three different controller design strategies to control the mechanical angular velocity of PMBLDC motor. Two of these strategies are P (proportional) and PI (proportional integral) controllers (Section 4.2 and Section 4.3) where the controller parameters are determined by investigation of the root locus of the linear model of the open loop system transfer function (obtained at Section 4.1). These strategies are straightforward but they give insight about the characteristics of the system. The third strategy is to use a FLC (Section 4.4). FLC also possess some parameters to be adjusted for better operation and these parameters are critical as they contribute the performance of the controller and overall system as well (Section 4.5). In these simulations the performance of the controllers are checked depending on four different indices. The first index is the of the steady state value of mechanical angler speed of the motor w_{m_ss} . w_{m_ss} is compared with the reference w_{m_ref} . The second one is maximum overshoot value os_{max} , the third one is the rise time t_r and the fourth one is the settling time value t_s .

The equations for system are given in the previous chapter. Using those equations we have constructed the SIMULINK model for the BLDC motor and in the SIMULINK model we used the parameters shown on Table 2.

Table 2: BLDC Motor Specification

Number of Phase	3(star)
Rated speed	4228 rpm (442.7551 rad/sec)
Rated current	6.8 A
Number of poles	8
Moment of inertia (J)	0.000019 Nm-s ²
Voltage constant (K _e)	0.0419 V/rad/s
Torque constant (K _t)	0.0419 Nm/A
Stator equivalent resistance (R)	0.348 Ω
Stator equivalent inductance (L)	0.000314 H

4.1 Obtaining the Linearized Open Loop Model of the System

In order to synthesize controllers with outstanding performance, obtaining the open loop transfer function of the linear model of the system is the starting point. For this reason we have to find an approximate open loop transfer function of PMSM motor which is indeed non-linear. To achieve this goal we have to find the input-output relation where the input of the open loop system is the reference current value I_{max} (it is taken a unit step function whose initial value is 0 Ampere and final value is the rated current value of 6.8 Ampere) and the output is the ω_m (the mechanical speed of the motor). While finding this input-output relation we haven't connected controllers hence the system become open loop. The parameters of the model are taken as $V_{dc}=40$ Volt and $T_L=0$ Nm. In these circumstances, the open loop model of the system is simulated. When steady-state conditions are reached in the simulation we have nearly obtained an angular mechanical speed value close to the rated speed value (4228 rpm), which means we obtain an approximated model of the PMSM motor. Mechanical angular speed versus the time graph of the open loop system is given in Figure 16 (the blue plot).

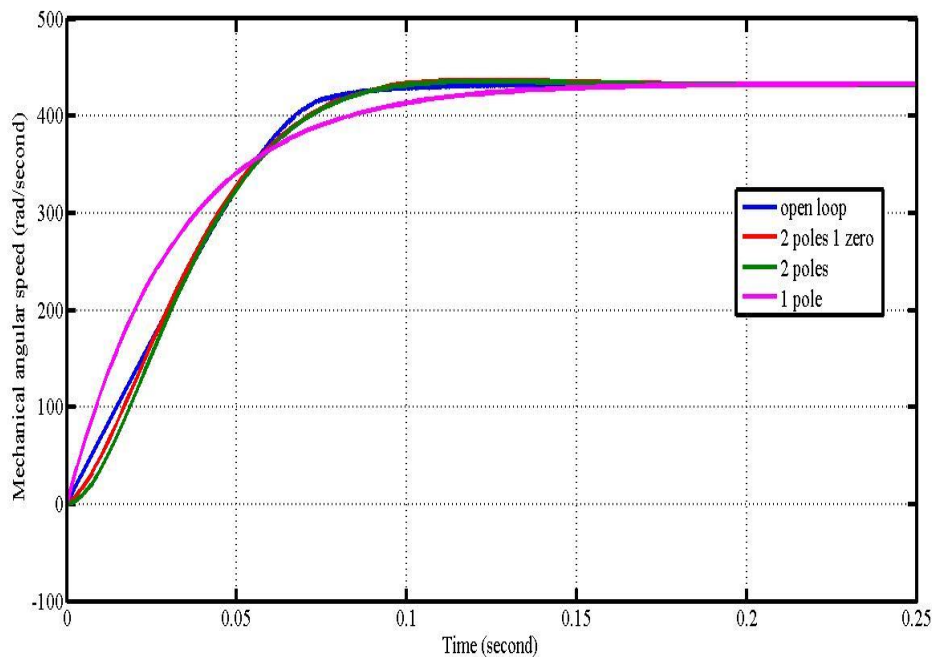


Figure 16 The mechanical speed of the open loop system and the approximated systems.

After this step we want to obtain an approximate transfer function of this system. For this purpose we used System Identification Toolbox of MATLAB. We decided check 3 different alternatives. The first alternative is a transfer function with 2 poles and 1 zero, the second alternative is a transfer function with only two poles and the third alternative is a transfer function with only a single pole. Using the input-output data of the actual system, we obtained the transfer functions of approximated linear systems for three alternative. The transfer functions of these three alternatives are as follows:

$$\text{Alternative 1: } tf_1 = \frac{331.7s + 1.253 \cdot 10^5}{s^2 + 73.155s + 1971}$$

The poles and zero of this transfer function are as follows:

Poles = $-36.5760 + j25.1566$ and $-36.5760 - j25.1566$

Zero = -377.8029

$$\text{Alternative 2: } tf_2 = \frac{1.391 \cdot 10^5}{s^2 + 78.45s + 2188}$$

The poles of this transfer function are as follows:

Poles = $-39.2250 + j25.4772$ and $-39.2250 - j25.4772$

$$\text{Alternative 3: } tf_3 = \frac{1974}{s + 30.98}$$

The pole of this transfer function is:

Poles = -30.98

After finding these alternative transfer functions, we have applied a unit step input with a magnitude of 6.8 (this is the rated current value) to each of them and obtained the corresponding outputs (mechanical angular velocities). The corresponding angular velocities as a function of time are also shown in Figure 16. As can be observed from the plots the best approximation to actual open loop response is the response, which is obtained using the alternative 1. Hence in order to design our controller we decided to use the alternative 1. We have chosen tf_1 as our linear plant model.

4.2 PI Controller Design: Root Locus Method

We first decided to use root locus method. Root locus method allows us to find the poles and zeros of the closed loop system when a P, PI or PID controller is used. Our approach is as follows:

First obtained the root locus plot of the linear plant model (for alternative 1). The root locus plot is shown in Figure 17.

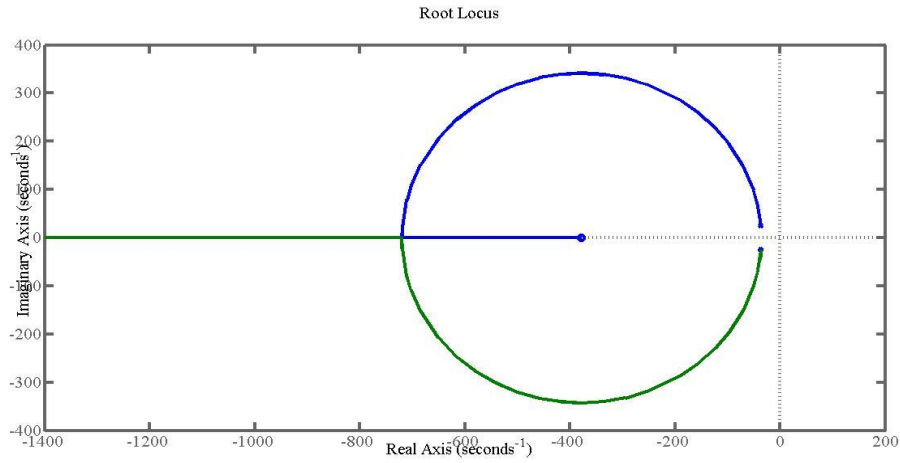


Figure 17 The root locus plot of approximated system at the first alternative.

Checking the root locus plot of the approximated system we decided to use a controller with a single pole and a single zero. The location of the pole of the controller is chosen at the origin and the location of the zero is chosen very close to the zero of the approximated system. Hence we decided the transfer function of the controller as:

$$tf_{controller} = \frac{s+377}{s}$$

By multiplying the controller transfer function and the linear plant transfer functions we obtained the total control + plant transfer function as

$$tf_{total} = tf_1 \times tf_{controller} = \frac{331.7s^2 + 2.504 \cdot 10^5 s + 4.724 \cdot 10^7}{s^3 + 73.15s^2 + 1971s}$$

Now we have to obtain the root locus plot of tf_{total} . The root locus plot of tf_{total} is shown in Figure 18.

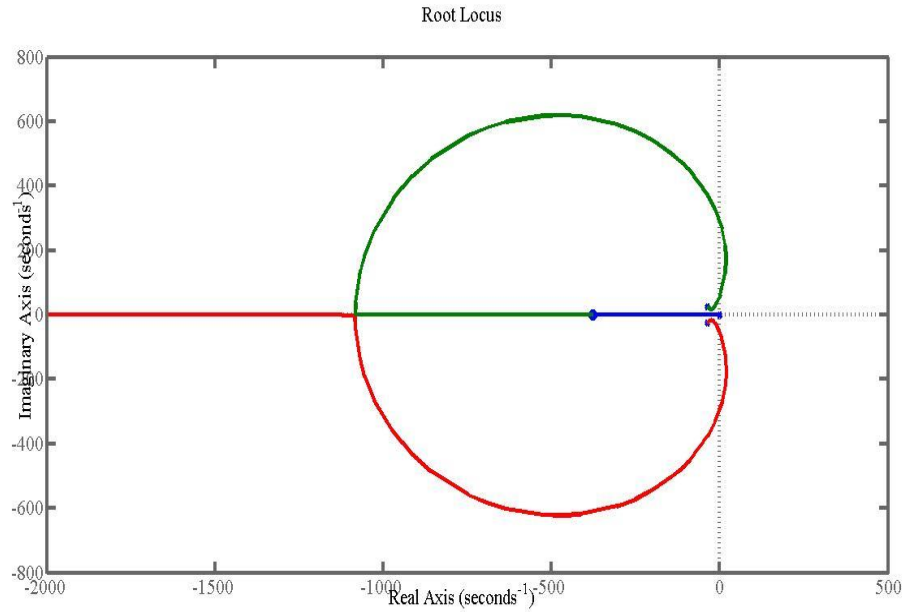


Figure 18 The root locus plot of the total open loop system together with controller.

Now we can determine the parameter of our PI controller. The PI controller transfer function is of the form

$$tf_{PI} = K\left(P + \frac{I}{s}\right) = K\left(\frac{sP + I}{s}\right)$$

We obtain $P=1$ and $I=377$ trivially by equating the pole and zero of $tf_{controller}$. Hence we determined the P and I parameters of PI controller. However we have to select a gain value K such that the overall system is not oscillatory and as fast as possible as well. So to determine this gain value we should choose a suitable working point on the root locus plot from Figure 18. Generally this working point is chosen as a point close to the intersection points of poles in root locus. A gain value $K=7.19$ results with poles at the locations $p_{1,2} \cong -1.08 \times 10^3$ and $p_3 \cong -289$.

Using these values we have constructed our PI controller. The reference value of the motor mechanical angular speed is determined as 400 rad/sec and the closed loop system is simulated under these conditions with $V_{dc}=68$ Volt and $T_L=0.5$ Nm. The motor mechanical speed as a function of time is shown in Figure 19.

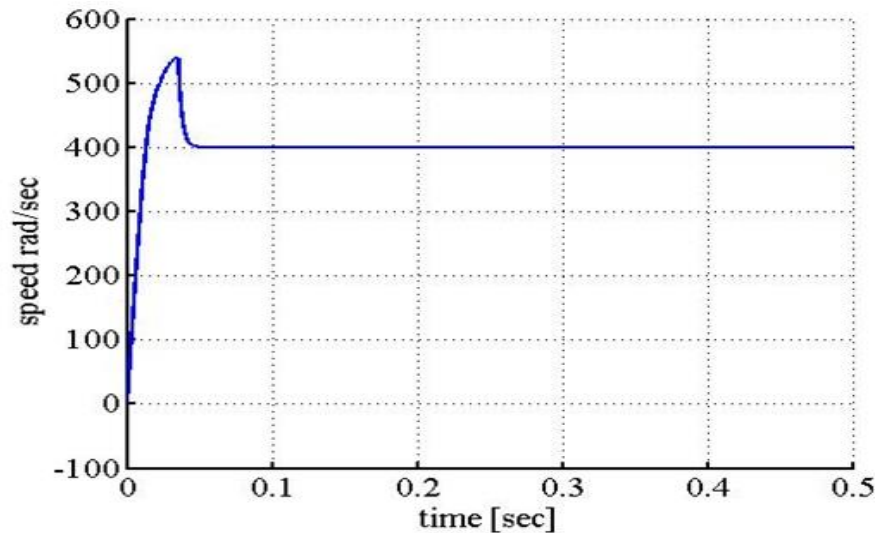
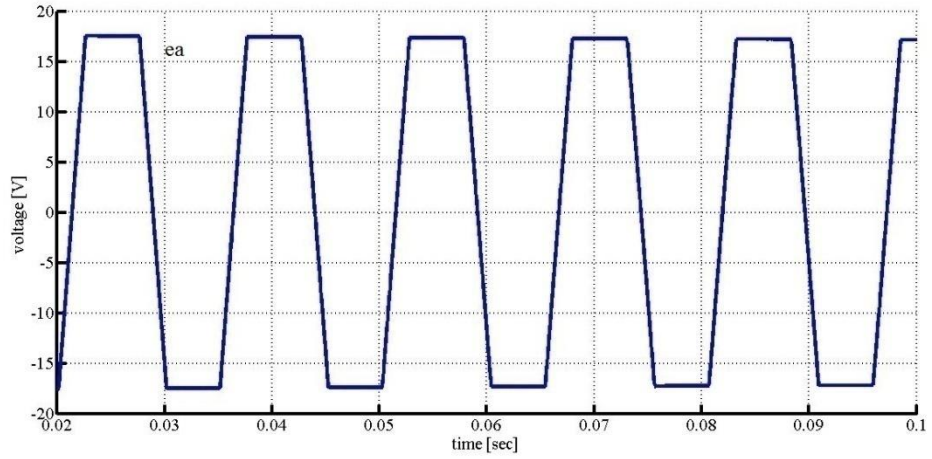


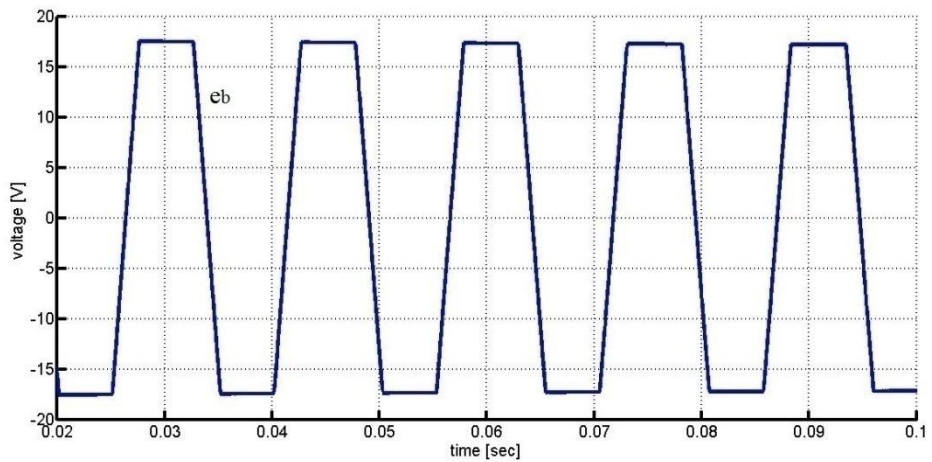
Figure 19 The mechanical speed of the motor as a function of time

As we deeply investigate Figure 19, we observe that the steady state value of the mechanical angular speed of the motor (w_{m_ss}) reaches to 400 rad/sec. However the response has very huge overshoot since the mechanical angular speed of the motor reaches to a maximum value of 541.54 rad/sec value (w_{m_peak}) which exceeds the steady state value by 35.385 %. The rise time t_r (the time passed for the motor to reach to the steady state value for the first time) is nearly equal to 0.0131 seconds. One of the drawbacks of the PI controller is since it creates an overshoot it takes long time to settle the response to the steady state value hence the settling time of the response shows poor performance. From deeper analysis of the Figure 19 we also observed that the mechanical angular velocity of the motor remains between 400 and 408 rad/sec (nearly %2 tolerance band compared to the w_{m_ss}) after a settling time (t_s) duration of 0.0424 seconds. Hence it takes long duration for the response to reach to the steady state value.

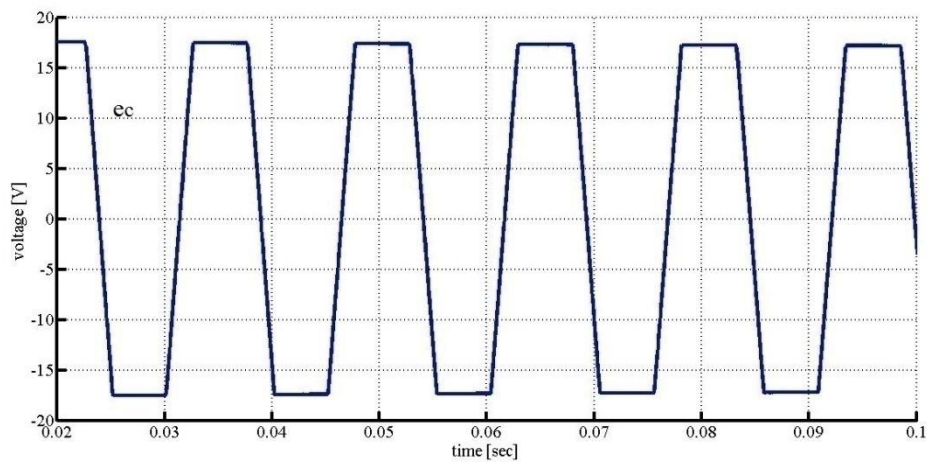
In Figure 20 the back-EMF waveforms (e_a , e_b , e_c) generated at 400 rad/s are shown. The amplitude of the back-EMF is 17.78 V. As seen each waveform has 120 degrees phase difference with the other waveforms.



(a)



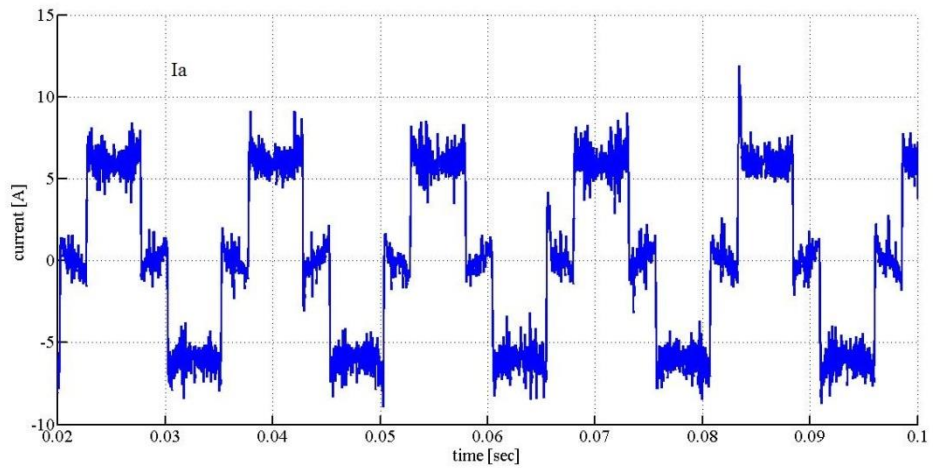
(b)



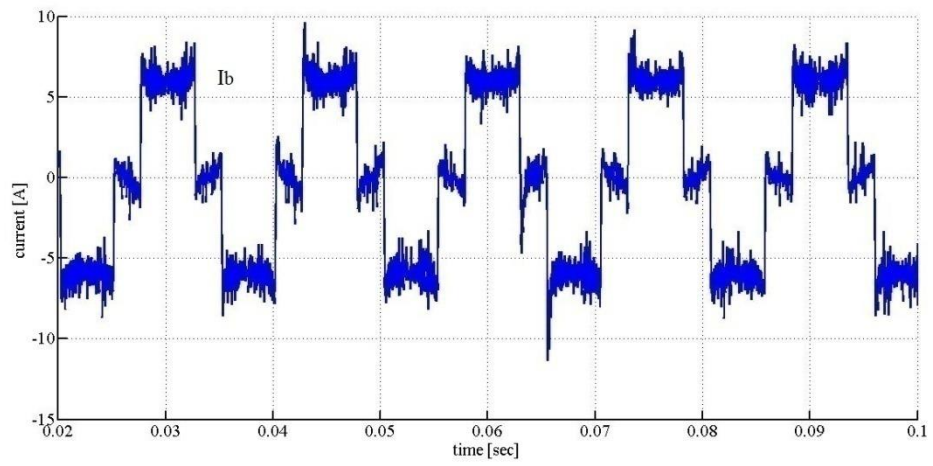
(c)

Figure 20 Back-EMF waveforms for Phases A, B and C respectively

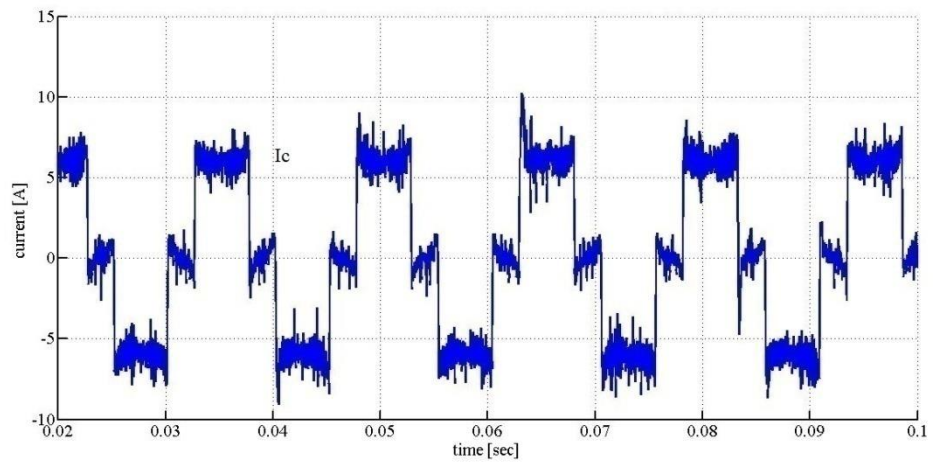
In Figure 21, the phase current waveforms are shown. As seen the phase are synchronized with back-EMF waveforms.



(a)



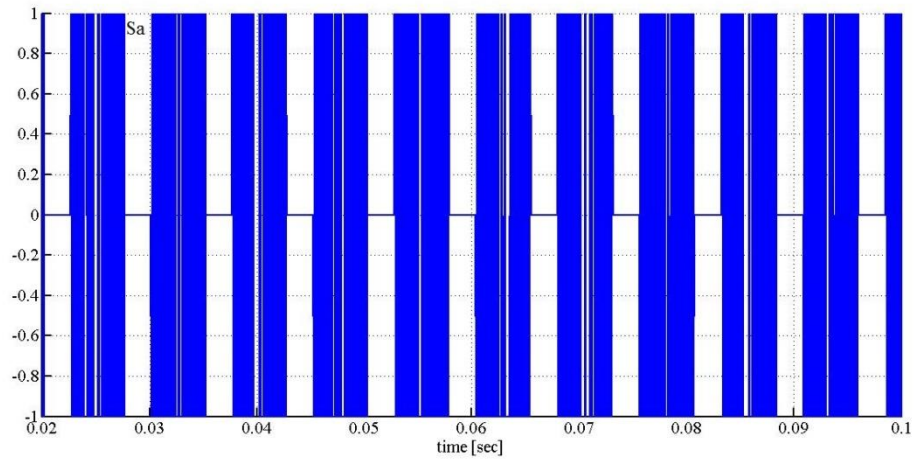
(b)



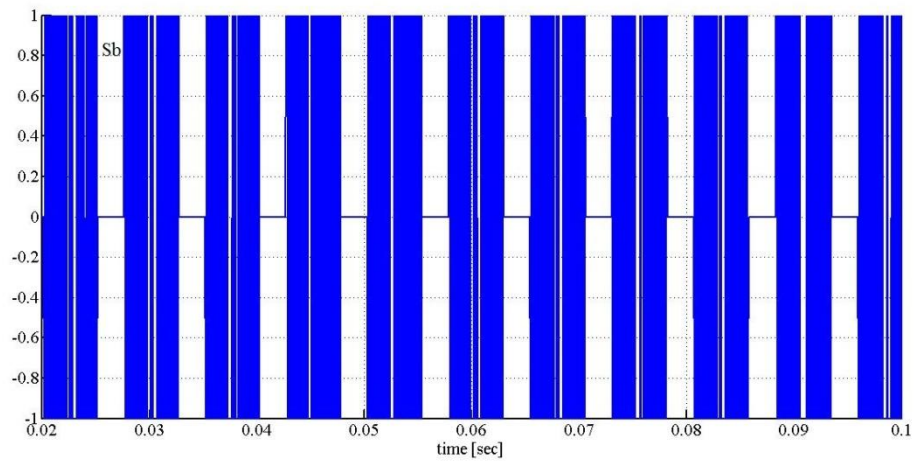
(c)

Figure 21 Phase currents waveforms for phase A, B and C respectively

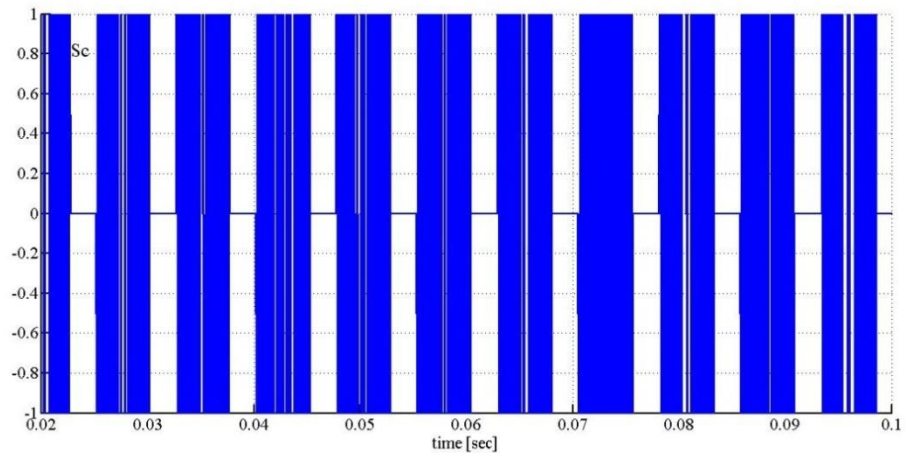
In Figure 22 we observe the switching characteristics of PWM inverter circuits for each phase. There is 120 degrees phase shift between the switching function signal. The positive (1) and negative (-1) values of the switches represent polarity of the applied DC voltage source V_{dc} . By the help of these switching characteristics we obtain the line-to-line voltage waveforms V_{ab}, V_{bc}, V_{ca} . These waveforms are shown in Figure 23.



(a)

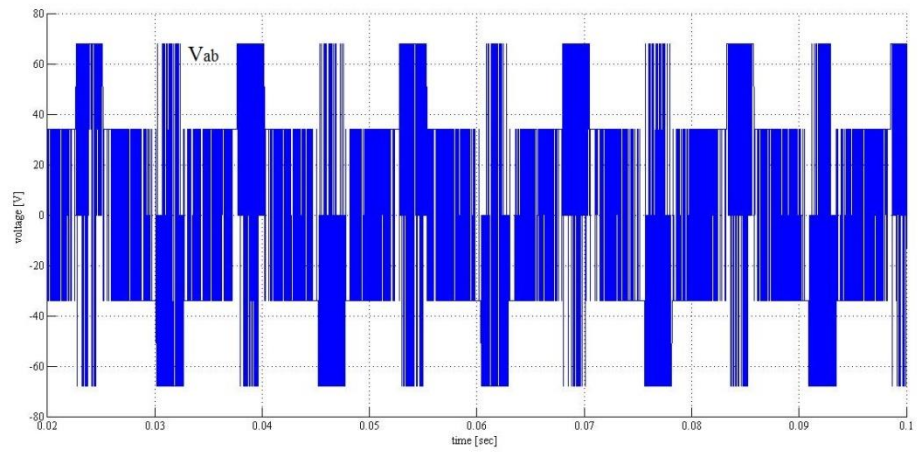


(b)

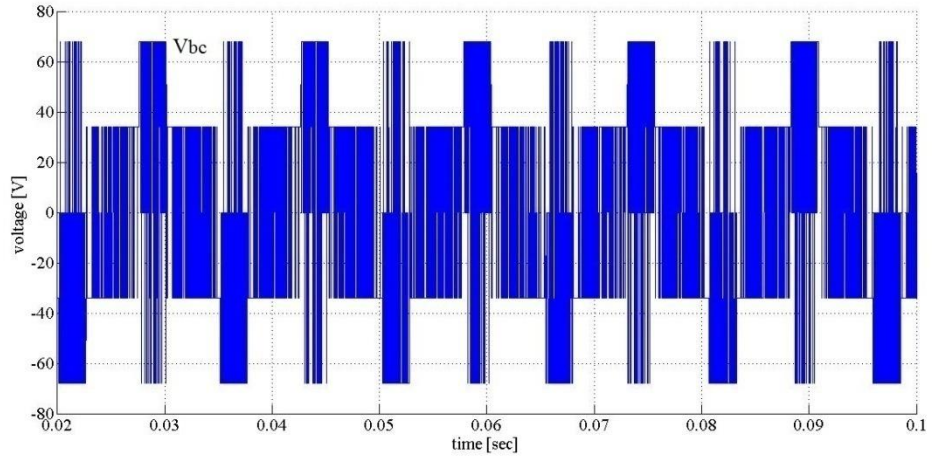


(c)

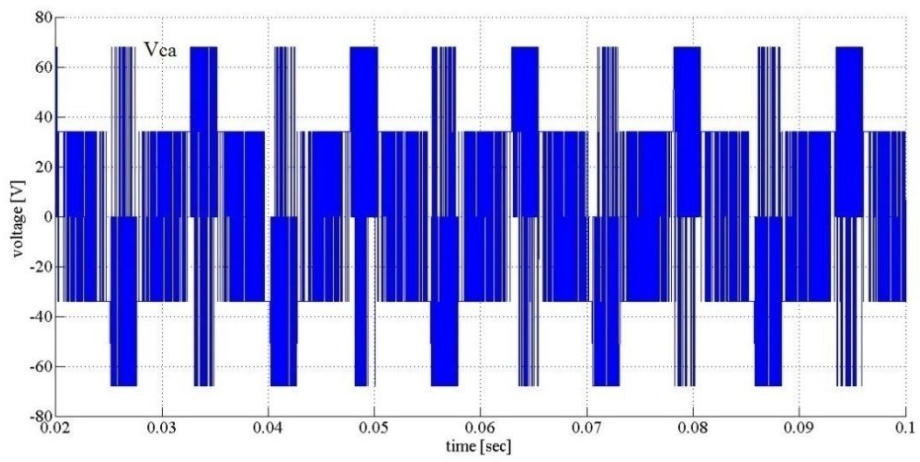
Figure 22 Switching function for Phase a, b and c respectively



(a)



(b)



(c)

Figure 23 Line-to-line voltages V_{ab} , V_{bc} , and V_{ca} respectively.

In Figures 24 and 25 the equivalent torque and the maximum current (I_{max}) graphs as a function of time are shown respectively.

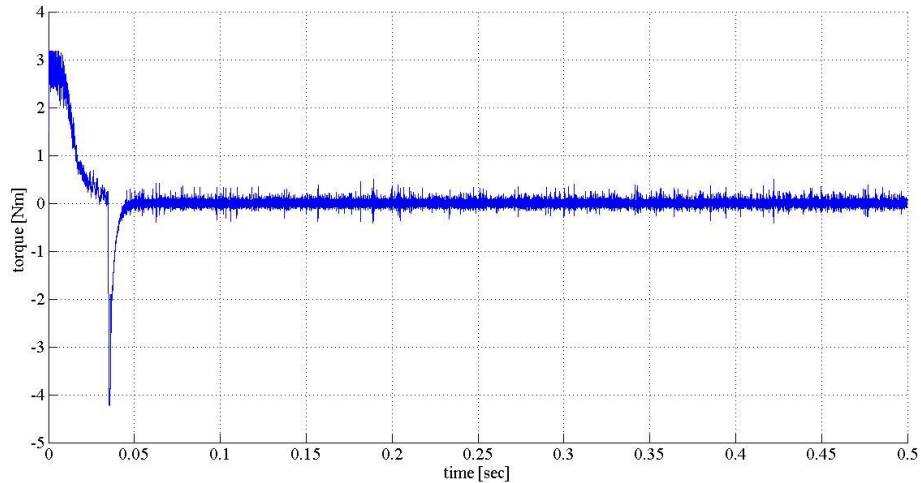


Figure 24 Equivalent torque of BLDC motor

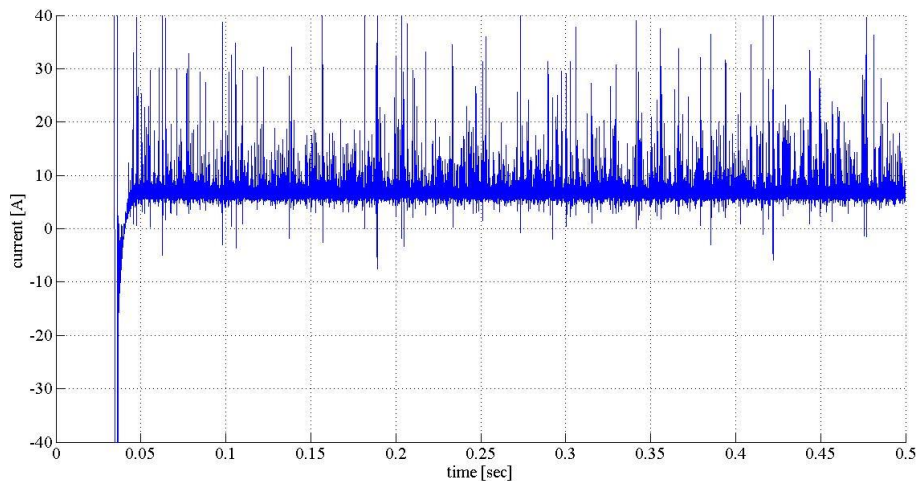


Figure 25 Max current of BLDC motor (I_{max})

4.3 P Controller Design: Root Locus Method

Instead of a PI controller we want to see the effect of P controller. In order to obtain the proportional gain value we use some critical information that we obtain from the root locus graph of the linear plant shown in Figure 17. We want the system not to have any overshoot and besides the response should be as fast as possible. For this reason the gain value should be determined such that both of the poles of the closed loop system should be real and poles should be close to each other such that none of them are dominant. That is only possible at break-in breakaway point in the root locus plot. We observed that break-in breakaway point is reached when the gain value is 4.12. Besides at the break-in breakaway point the value of closed loop poles

are $p_{1,2} = -720$. Thus if P controller gain value is taken as 4.12 and $K=1$ there are no other controller parameters to be adjusted anymore ($I=0$, $D=0$). All the other parameters and procedures in the simulation are taken the same as PI simulation at section 4.2. As the result of the simulation the mechanical angular speed profile shown in Figure 26 is obtained.

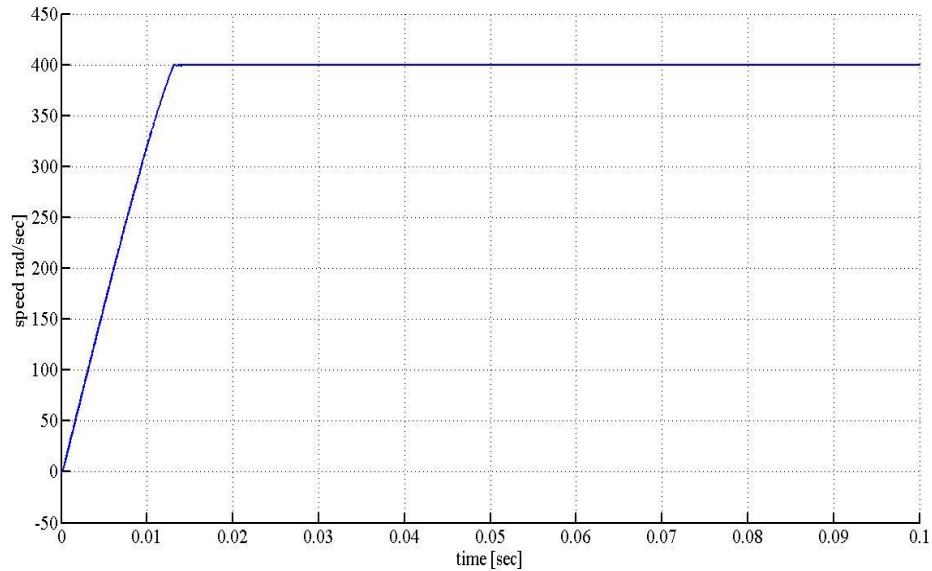


Figure 26 The mechanical speed of the motor as a function of time

As we deeply investigate Figure 26, we observe that w_{m_ss} reaches nearly to 399.94 rad/sec and besides the response has 0.11% os_{max} . It is also observed that the t_r is nearly equal to 0.0131 seconds and settling time t_s is 0.0127 seconds. An advantage of this controller compared to the PI controller in section 4.2 is even though there is much more steady state error compared to the simulation at section 4.2, the P controller in this simulation demonstrates a better settling time performance since it does not have big overshoot value.

The equivalent torque and the I_{max} graphs for this simulation are shown in Figure 27 and 28 respectively.

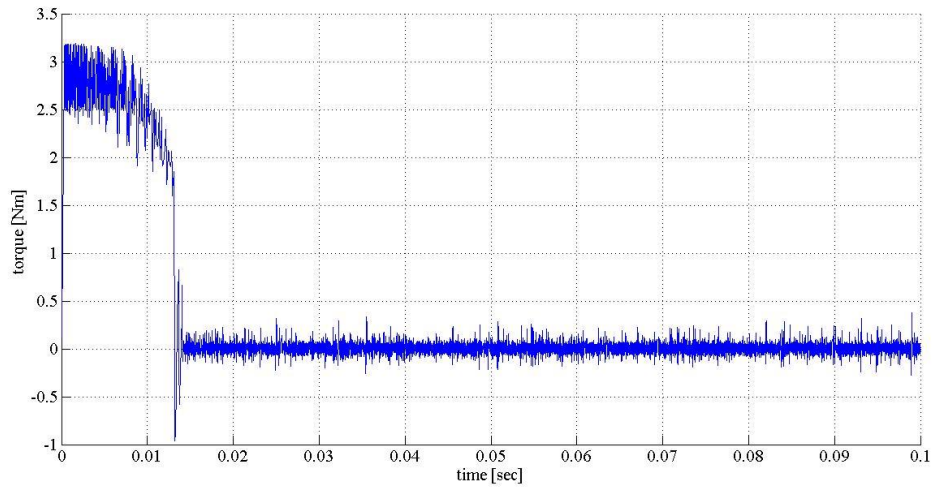


Figure 27 Equivalent torque of BLDC motor

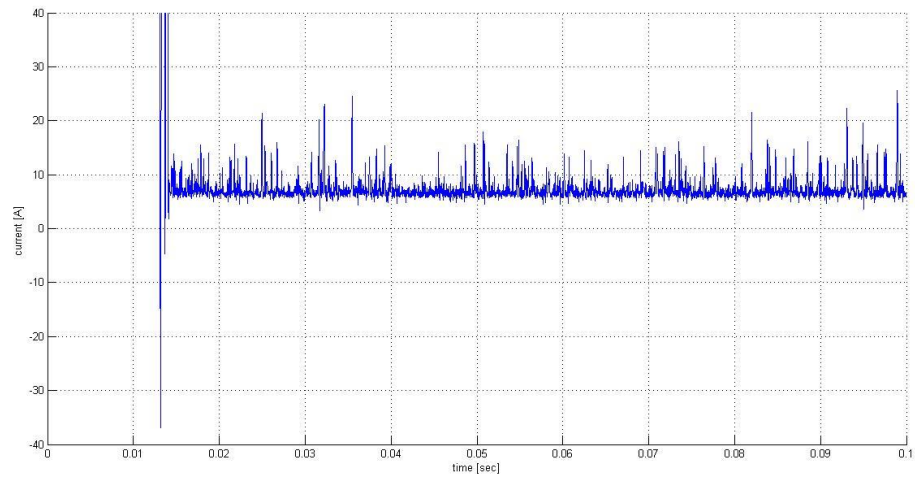


Figure 28 Max current of BLDC motor (I_{max})

4.4 FLC Controller

In this section instead of using P or PI controller we decided to use FLC to stabilize the BLCD motor speed. In order to see the efficiency of the FLC we used two different rule base structures. These rule base structures are given at Table 3 and 4. Each rule-base includes 49 rules.

Table 3: Rule of Fuzzy Logic control case1

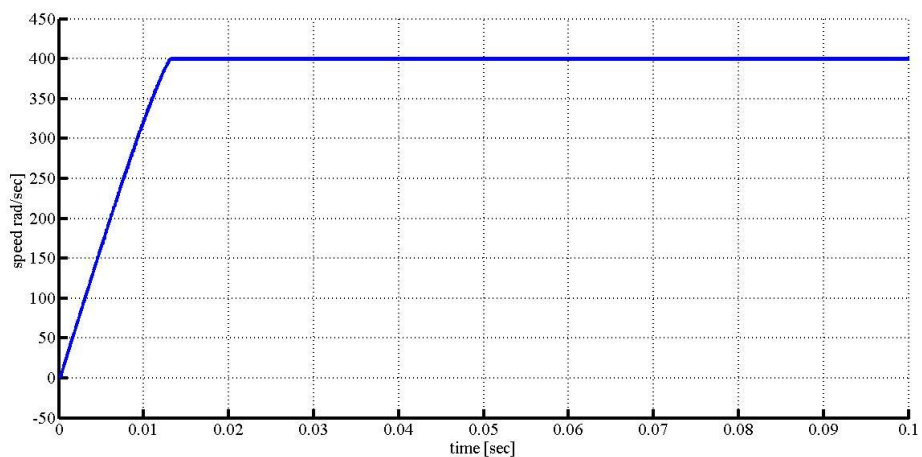
e_1 and e_2	PB	PM	PS	Z	NS	NM	NB
PB	PB	PB	PM	PM	PS	PS	Z
PM	PB	PM	PM	PS	PS	Z	NS
PS	PM	PM	PS	PS	Z	NS	NS
Z	PM	PS	PS	Z	NS	NS	NM
NS	PS	PS	Z	NS	NS	NM	NM
NM	PS	Z	NS	NS	NM	NM	NB
NB	Z	NS	NS	NM	NM	NB	NB

Table 4: Rule of Fuzzy Logic control case2

e_1 and e_2	PB	PM	PS	Z	NS	NM	NB
PB	PB	PB	PB	PM	PM	PS	Z
PM	PB	PB	PM	PM	PS	Z	NS
PS	PB	PM	PM	PS	Z	NS	NM
Z	PM	PM	PS	Z	NS	NM	NM
NS	PM	PS	Z	NS	NM	NM	NB
NM	PS	Z	NS	NM	NM	NB	NB
NB	Z	NS	NM	NM	NB	NB	NB

In Tables 3 and 4, the first row and the first column gives the linguistic variables assigned to the inputs of the FLC controller e_1 and e_2 . The other indices of the tables give the assignment of the output variable u . These two control strategies are indeed different kinds of sliding mode control schemes implemented using FLC.

In the first simulation the rule-base structure in Table 3 is used. The normalization factors are taken as $N_{e_1}=1/220$, $N_{e_2}=1/5000000$ and $N_u=1500$. As the result of the simulation the mechanical angular speed profile shown in Figure 29 is obtained.

**Figure 29** Mechanical speed of FLC case1

From Figure 29, we obtained the following performance indices:

There is no overshoot in the response, $t_r=0.0131$ second, $w_{m_ss}=399.85$, $t_s=0.0127$. The equivalent torque and the I_{max} graphs for this simulation are shown in Figure 30 and 31 respectively.

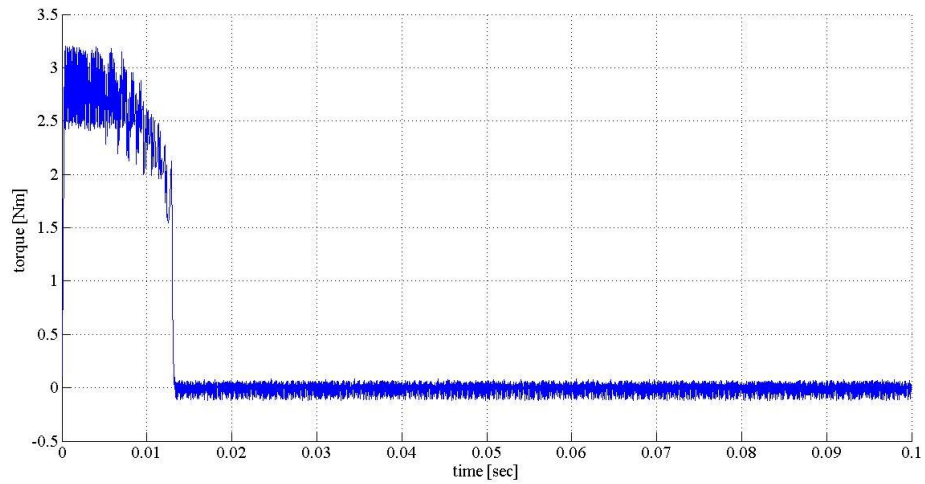


Figure 30 Equivalent torque of BLDC motor for FLC case1

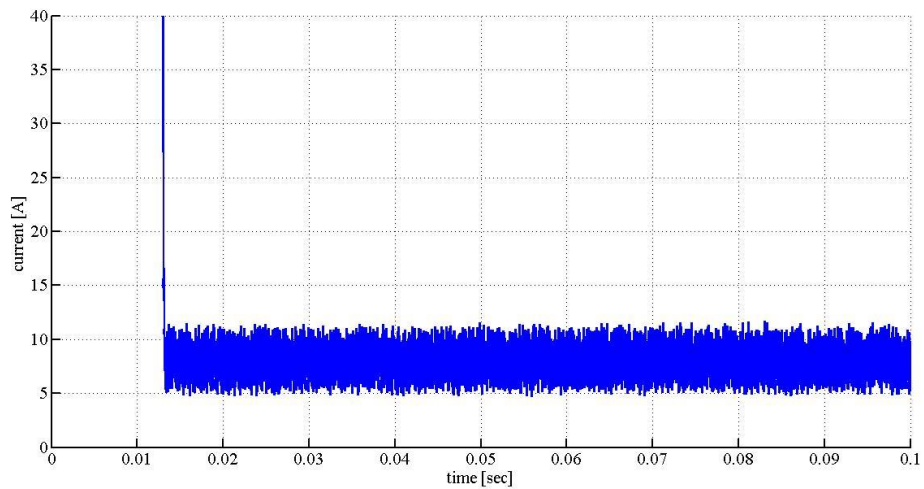


Figure 31 Max current of BLDC motor (I_{max}) of FLC case 1

In the second simulation the rule-base structure in Table 4 is used. The normalization factors are taken as $N_{e_1}=1/220$, $N_{e_2}=1/5000000$ and $N_u=1500$. As the result of the simulation the mechanical angular speed profile shown in Figure 32 is obtained.

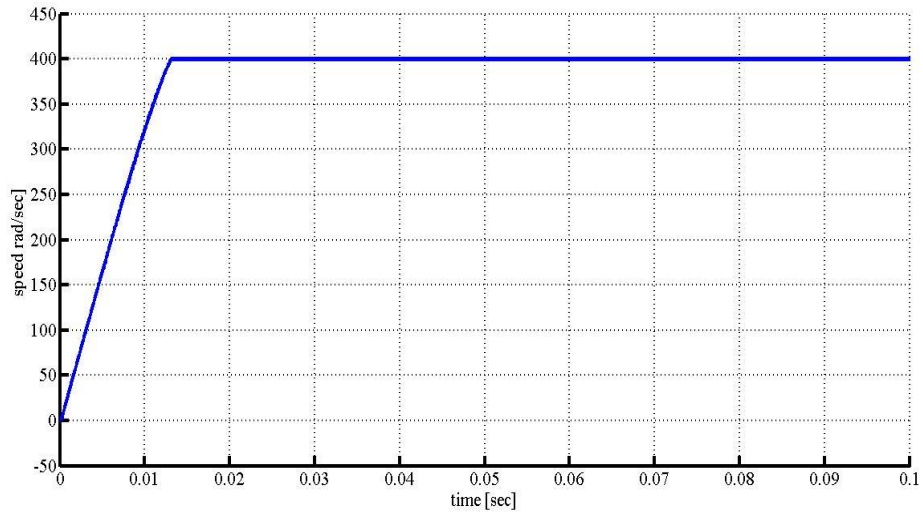


Figure 32 Mechanical Speed of FLC Case2

From Figure 32, we obtained the following performance indices:

There is no overshoot in the response, $t_r=0.0124$ second, $w_{m_ss}=399.91$, $t_s=0.0119$.

The equivalent torque and the I_{max} graphs for this simulation are shown in Figure 33 and 34 respectively. As we observe there is not so much difference between the performance indices of these two FLC simulations however the steady state value of the second simulation is slightly better the first simulation and the reference current value of the first simulation is better than the second one.

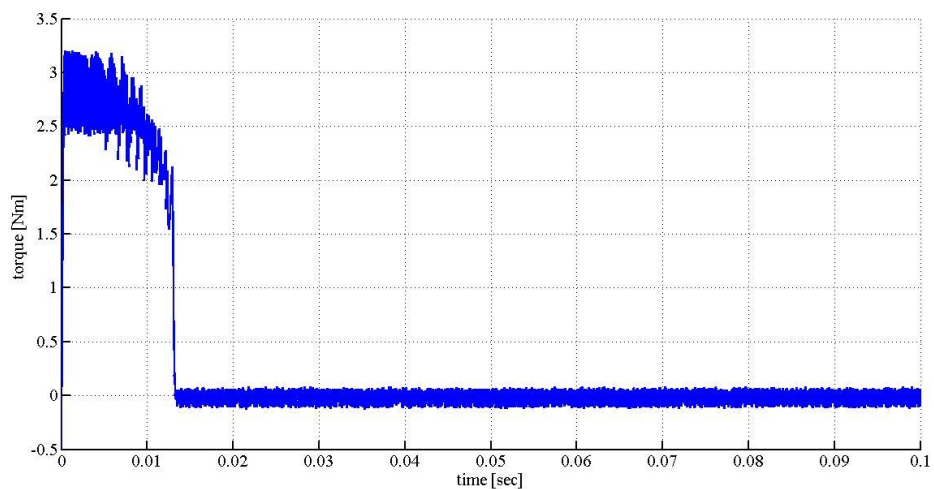


Figure 33 Equivalent torque of BLDC motor for FLC case2

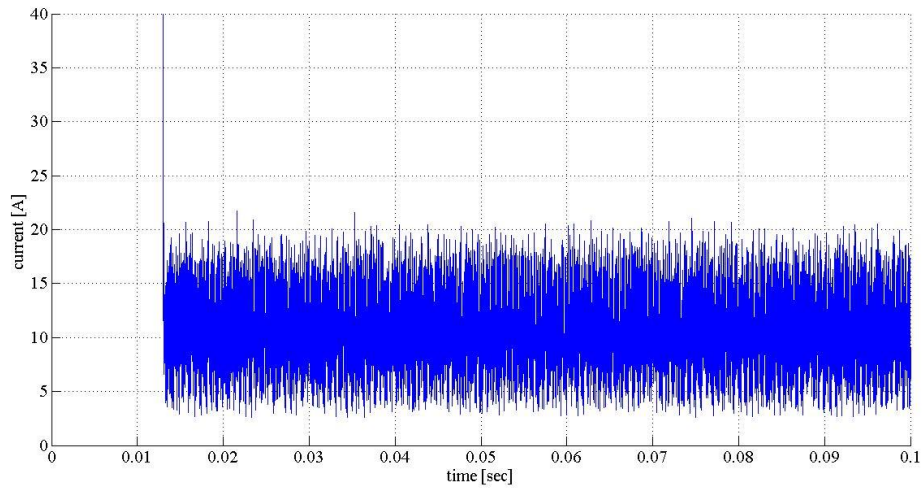


Figure 34 Max current of BLDC motor (I_{max}) of FLC case 2

4.5 Comparison of Controllers for Reverse Motor Operation

We also wanted to test the controllers. This time the reference value of the mechanical angular speed of the motor is determined as -400 rad/sec with $T_L=0.5$ Nm and $V_{dc}=68$ Volt. At these circumstances the following performance indices are obtained for the synthesized controllers.

Table 5: The performance indices of controllers for -400 rad/sec.

	PI controller	P controller	FLC controller Case 1	FLC controller Case 2
w_{m_ss} (rad/sec)	-400.01	-400.05	-400.07	-400.01
t_r (second)	9.91×10^{-3}	9.91×10^{-3}	0.0101	0.0101
t_s (second)	0.0292	9.667×10^{-3}	9.666×10^{-3}	9.666×10^{-3}
OS_{max} %	50	0.26	Not available	Not available

As seen from Table 5, except PI controller all controllers have good performance indices.

4.6 Comparison of Controllers for Small Reference Changes

Another test for the performance of the controllers is checking the performance indices for small reference point changes. For this reason, two different applications are carried out. In the first application the reference mechanical angular speed of the motor is set to 20 rad/sec while the initial mechanical angular speed of the motor is set to 0 rad/sec with $T_L=0.5$ Nm and $V_{dc}=68$ Volt. At these circumstances the

following performance indices are obtained for the synthesized controllers (at Table 6):

Table 6: The performance indices of controllers for reference changes at lower speeds

	PI controller	P controller	FLC controller Case 1	FLC controller Case 2
w_{m_ss} (rad/sec)	20	19.94	19.885	19.95
t_r (second)	7.44×10^{-4}	7.43×10^{-4}	7.79×10^{-4}	7.635×10^{-4}
t_s (second)	627×10^{-3}	1.432×10^{-3}	7.79×10^{-4}	9.357×10^{-4}
OS_{max} %	30	7.0211	1.3151	4.1103

In the second application, the reference mechanical angular speed of the motor is set to 400 rad/sec while the initial mechanical angular speed of the motor is set to 380 rad/sec with $T_L=0.5$ Nm and $V_{dc}=68$ Volt. As seen the difference between the first and the second application is the speed range. The first application is carried out in order to exhibit the efficiency of the controllers for lower speeds whereas the second application is done for the same task at higher speeds. At these circumstances the following performance indices are obtained for the synthesized controllers (at Table 7):

Table 7: The performance indices of controllers for reference changes at higher speeds

	PI controller	P controller	FLC controller Case 1	FLC controller Case 2
w_{m_ss} (rad/sec)	400	399.93	399.85	399.92
t_r (second)	1.1735×10^{-3}	1.181×10^{-3}	1.5×10^{-3}	1.44×10^{-3}
t_s (second)	2.8975×10^{-3}	1.915×10^{-3}	1.5×10^{-3}	1.44×10^{-3}
OS_{max} %	29.25	1.8063	0	0

As seen from Table 6 and Table 7, The FLCs are more successful compared to P and PI controllers.

CHAPTER 5

CONCLUSION

Recently, BLDC motors are replacing DC motors in different industrial application. Hence there is a requirement for deeper analysis of these kinds of motors. One of the areas the researches are focusing is the control of these motors under desired conditions. For better controller synthesis the linear model for BLDC motor is necessary. For this purpose a MATLAB/SIMULINK model for BLDC motor drives is implemented in this thesis. The model of the BLDC motor is non-linear and it was also obtained in previous studies. What is different and new compared to the previous studies in this thesis is the synthesis of the linear plant model based on the step response of the system under rated current conditions. Once the linear approximated model of the plant is obtained, it is easy to implement more effective controllers for mechanical angular speed control of BLDC motors. Depending on this linear plant we proposed two PID controllers (PI and P controllers). We compared the PI and P controllers with a strong FLC controller with two different rule-base settings that resemble a sliding mode control strategy.

In the simulations many different dynamic characteristics such as mechanical angular velocity, phase and line voltages, the reference current, mechanical torque, back-EMF and phase currents are also observed. Besides the controllers are checked in terms of performance indices (steady state value, maximum overshoot, rise time, settling time) related with the mechanical angular velocity of the motor. FLC controller show good performance but it should also be pointed out that P controller whose parameters are determined by root locus is also very successful. Surprisingly, PI controller is not very successful. We think this happens due to integrator windup. The controller and plant system in Section 4.2 has an integrator and this system is excited by a step input. In this case the system behaves slower compared to controller and the sudden changes in the error began to accumulate and the control signal

saturates. This has caused a very big overshoot for mechanical angular speed in Section 4.2.

The future plans related to this study are investigating the means of increasing the FLC controller performance by optimization and by application of new rule-base structures, synthesis of new controller using other conventional controller synthesis techniques and using the models obtained in the thesis for torque control.

REFERENCES

1. **Kumar J.S., Joice S.R., (2011),**“*Practical Implementation of Four Quadrant Operation of Three Phase Brushless DC Motor using dsPIC*”,pp.91-94.
2. **Krishnan R., Beutler A.J., (1985),**“*Performance and Design of An Axial Field Permanent Magnet Synchronous Motor Servo Drive*”, in Proc. IEEE IAS Annu. Meeting, pp. 634-640.
3. **Mazenc M., Villanueva C., Hector J., (1985),**“*Study and Implementation Of A Hysteresis Controlled Inverter On A Permanent Magnet Synchronous Machine*”, IEEE Transaction on Industrial Applications, vol. IA-21 no.2, pp408-413.
4. **Hanselman D., (2006),**“*Brushless Permanent Magnet Motor Design*”, 2nd Edition, Magna Physics Publication, United States of America, pp. 1-226.
5. **Singh A.K., Kumar K., (2002),**“*Modelling and Simulation of PID Controller Type PMBLDC Motor*”, Proceedings of National Seminar on Infrastructure Development Retrospect and prospects Institution of Engineers (I),(India) , vol. 1, pp. 137-146.
6. **Jahns T. M., (1984),**“*Torque Production In Permanent-Magnet Synchronous Motor Drives With Rectangular Current Excitation*”, IEEE Trans. Ind. Appl., vol. 20, no. 4, pp. 803-813.
7. **Funabiki S., Himei T., (1985),**“*Estimation of Torque Pulsation Due To The Behavior Of A Converter And An Inverter In A Brushless Dc-Drive System*”, Proc. Inst. Elec. Eng., vol. 132, no. 4, pp. 215-222.
8. **Dwivedi A. , Tiwari A., (2013),**“*A Review : Speed Control of Brushless DC Motor*”, *IJBSTR*, vol. 1, no. 6, pp. 14–19.
9. **Zhong L., Rahman M., Lim K., (1997),**“*Analysis of Direct Torque Control In Permanent Magnet Synchronous Motor Drives*”, *IEEE Transactions on Power Electronics*, vol. 12, pp. 528-536.

10. **Rambabu S., (2007)**, “*Modeling And Control of A Brushless Dc Motor*”, M.S. Thesis, National Institute of Technology, Rourkela.
11. **Gambhir R., Jha A., (2013)**, “*Brushless DC Motor : Construction and Applications*”, *Int. J. Eng. Sci.*, vol. 2, no. 5, pp. 72–77.
12. **Lee B., Ehsani M., (2003)**, “*Advanced Simulation Model for Brushless DC Motor Drives*”, *Electric Power Components and Systems*.vol. 31, 841–868.
13. **Sing B., Reddy A.H.N., Murthy S.S., (2003)**, “*Gain Scheduling Control of Permanent Magnet Brushless dc Motor*”, *IE(I) Journal-EL*, vol. 84, 52-62.
14. **Lee B.K, Ehsani M.A., (1999)**, “*Simplified Functional Model For 3-Phase Voltage-Source Inverter Using Switching Function Concept*”, *IEEE Trans. on Industrial Electronics*, vol.1, pp.462-467.
15. **Salazar L., Joos G., (1994)**, “*PSPICE Simulation Of Three-Phase Inverters By Means Of Switching Functions*”, *IEEE Trans. on Power Electronics*, vol. 9, no. 1, pp. 35–42.
16. **Kuklee B., Ehsani .M, (2003)**, “*Advanced Simulation Model for Brushless DC Motor Drives Electric Power Components and Systems*”, vol. 31,no.9, 841-868.
17. **Rubai A., Ofoli A, Castro M., (2006)**, “*DSP-Based Rapid Prototyping of Fuzzy PID Controls for High Performance Brushless Servo Drives*”, *IEEE Industry Applications Conference, 41st IAS Annual Meeting*, pp.1360–1364.
18. **Kim T., Park B., Lee D., Ryu J., Hyun D., (2008)**, “*A New Approach To Sensorless Control Method For Brushless DC Motors*”, *International Journal of Control, Automation, and Systems*, vol. 6, pp. 477-487.
19. **Hemch I., (2013)**, “*Mathematical Modeling and Position Control Of Brushless Dc (BLDC) Motor*”, vol. 3, no. 3,pp.1050-1057
20. **Astorn k., hagglund T., (1994)**, “*PID Controllers Theory Design and Tuning*”, United States of America, p.54.
21. **Singh C. P., Kulkarni S., Rana S.C., (2013)**, “*Scientists State-Space Based Simulink Modeling of BLDC Motor and its Speed Control using Fuzzy PID Controller*”, *International Journal of Advances in Engineering Science and Technology*, vol. 2 , no. 3,pp.359-369.

22. **Lee C., (1990)**, *"Fuzzy Logic in Control Systems, Fuzzy Logic Controller, Parts I and II"*, IEEE Trans. Syst., Man, Cyber. vol. 20, pp. 404-435.
23. **Ali M., Aydin C., (2002)**, *"An Educational Tool For Fuzzy Logic Controlled BDCM"*, IEEE transaction on educational vol.45.no.1.
24. **Akçayol M., Aydin C., (2002)**, *"Design Of Fuzzy Speed Control Of The Brushless Dc Motor"*, IEEE transaction on education, vol.45.no.1.
25. **Ricketts D. , Kankam M., (2002)**, *"Development And Implementation of An Adaptive Fuzzy-Neural-Network Controller for Brushless Drives"*, IEEE Industry Applications Society, USA, vol.38, no.2.

APPENDICES A

CURRICULUM VITAE

PERSONAL INFORMATION

Surname, Name: IBRAHIM, Rafid Ali
Date and Place of Birth: 07 May 1970, Kirkuk
Marital Status: Married
Phone: 90 535 649 13 71 / +964 770 234 12 48
Email: Ibrahim_aslanuz@yahoo.com



EDUCATION

Degree	Institution	Year of Graduation
M.Sc.	Çankaya University, Electronic and Communication Engineering	2015
B.Sc.	Technical college in Kirkuk, Electronic and control Engineering, Iraq	2010
High School	11 athar Preparatory School	1999

FOREIGN LANGUAGES

Arabic, English, Turkish